Flame Propagation of Hydrogen Combustion

Jennifer Lorena Schurr

School of Engineering

Thesis submitted for examination for the degree of Master of Science in Technology.
Espoo July 4, 2022

Supervisor

Prof. Martti Larmi (Aalto)
Assoc. Prof. Justin Chiu (KTH)

Advisor

Dr. Ossi Kaario
Dr. Qiang Cheng
MSc. Maryam Yeganeh

Aalto University
School of Engineering

Aalto University
School of Engineering

Aalto University, P.O. BOX 11000, 00076 AALTO
www.aalto.fi
Abstract of the master's thesis

Author Jennifer Lorena Schurr

Title Flame Propagation of Hydrogen Combustion

Degree programme Innovative Sustainable Energy Engineering

Major Bioenergy **Code of major** ISEE

Supervisor Prof. Martti Larmi (Aalto)
Assoc. Prof. Justin Chiu (KTH)

Advisor Dr. Ossi Kaario
Dr. Qiang Cheng
MSc. Maryam Yeganeh

Date July 4, 2022 **Number of pages** 57+9 **Language** English

Abstract

In recent years the urge to make future fuels market ready and understand their potentials and risks has become considerably higher. Hydrogen as one of a limited number of zero emission fuels is getting more interesting in terms of supporting the energy transition.

This Master Thesis helps to understand hydrogen's combustion behaviour and flame propagation and if hydrogen has a future in the transportation industry. The thesis is conducted beginning with a literature study of previous laminar flame speed measurements, continues with 1D flame simulations in Cantera and finishes with optical flame speed measurements (Z-Schlieren) in a constant volume chamber. The flame propagation, the flame speed and its influencing factors, temperature, pressure and dilution, have been examined.

The results obtained by the simulations and experimental work have been validated, analysed and compared to literature. It could be displayed that the simulations and experiments vary since turbulences and uncertainties are affecting the accuracy of the system. In conclusion it shows that hydrogen has a high potential as future fuel but it is also to mention that future studies are required to give a fully educated statement.

Keywords Hydrogen, Combustion, Laminar Burning Velocity, Flame Propagation, Flame Speed, Optical Measurements, Cantera Simulations

Aalto University
School of Engineering

Aalto-universitetet, PB 11000, 00076 AALTO
www.aalto.fi
Sammandrag av diplomarbetet

Författare Jennifer Lorena Schurr

Titel Flame Propagation of Hydrogen Combustion

Utbildningsprogram Innovative Sustainable Energy Engineering

Huvudämne Bioenergy **Huvudämnets kod** ISEE

Övervakare Prof. Martti Larmi (Aalto)
Assoc. Prof. Justin Chiu (KTH)

Handledare Dr. Ossi Kaario
Dr. Qiang Cheng
MSc. Maryam Yeganeh

Datum July 4, 2022 **Sidantal** 57+9 **Språk** Engelska

Sammandrag

Under de senaste åren har behovet av att göra framtidens bränsle redo för marknaden och förstå deras potential och risker ökat avsevärt. Vätgas, som ett av ett begränsat antal nollutsläppsbränslen, blir alltmer intressant när det gäller att stödja energiomställningen.

Detta examensarbete bidrar till att förstå vätgasens förbränningsbeteende och flamspridning samt om vätgas har en framtid inom transportindustrin. Uppsatsen inleds med en litteraturstudie av tidigare mätningar av laminär flamhastighet, fortsätter med 1D-flamsimuleringar i Cantera och avslutas med optiska mätningar av flamhastighet (Z-Schlieren) i en konstantvolymkammare. Flammans utbredning, flamhastighet och dess påverkande faktorer, temperatur, tryck och utspädning, har undersökts.

De resultat som erhållits genom simuleringarna och det experimentella arbetet har validerats, analyserats och jämförts med litteraturen. Det kan konstateras att simuleringar och experiment varierar eftersom turbulens och osäkerheter påverkar systemets noggrannhet. Sammanfattningsvis visar det sig att vätgas har en stor potential som framtida bränsle, men det bör också nämnas att det krävs framtida studier för att kunna ge ett heltäckande utlåtande.

Nyckelord Vätgas, Förbränning, Laminär Förbränningshastighet, Flamspridning, Flamhastighet, Optiska Mätningar, Cantera Simulering

Preface

I want to thank the entire Energy Conversion Team of Aalto University for their general support and welcoming behaviour. I would like to specially mention Professor Martti Larmi who was willing to function as my supervisor from Aalto University side and my Co-supervisor Associate Professor Justin Chiu from KTH. A special thanks goes also to my advisors Ossi Kaario, Qiang Cheng and Maryam Yeganeh, who supported me with their expertise and guidance. I would like to express my gratitude to Olli Ranta, who helped me with the optical measurements and experimental setup. Thanks to Atmadeep Bhattacharya and his input and knowledge about the Cantera Simulations. The subject was challenging but very exciting and it is especially rewarding to be part of the future energy transition.

Otaniemi, July 4, 2022

Jennifer Lorena Schurr

Contents

List of Figures

List of Tables

Abbreviations

CH_4	methane
CO	carbon monoxide
CO_2	carbon dioxide
H_2	hydrogen
H_2O	water
LED	light emitting diode
N_2	nitrogen
N_2O	nitrous oxide
NH_3	ammonia
NO	nitrogen oxide
NO_x	nitrogen oxides
O_2	oxygen
OH	hydroxide
PM	particulate matter
SO_2	sulfur dioxide
T_{ad}	adiabatic flame temperature
UV	ultraviolet

1 Introduction

1.1 Motivation

Since the beginning of time combustion has been a major technology to produce energy. Even today, combustion is the most adopted technology to produce energy for heating, transportation and electricity. Also in the future, combustion will take an important role, for the combustion of renewable fuels to replace fossil fuels. This means, that it is of utmost importance to study and understand the combustion process. A central aspect of the combustion process and of this thesis is the flame, which can be laminar or turbulent.

The extraction of fossil fuel is releasing different kinds of emissions into the atmosphere. Acid runoffs and other toxic fluids contaminate water; heavy metals, radioactive materials, and other pollutants from fossil fuel mining generate wastewater; benzene and formaldehyde pollute the air around active oil and gas wells, as well as close to transport and processing facilities. In addition the combustion of fossil fuels releases even further emissions, not only with global warming potential and degradation of the ecosystem, but also with impact on human health. Emissions like particulate matter (PM), sulfur dioxide (SO_2), carbon monoxide (CO), carbon dioxide (CO_2) and nitrogen oxide (NO) [1].

In the last decades voices for sustainability have become considerably louder. When following political discussions governments and multinational organizations have participated in different climate conferences to establish climate goals and climate prevention action plans to mitigate the effect of human interactions on this planet. Even though each country agreed to specific terms to decrease the climate impact, CO_2 emissions are expected to continue rising. Due to the prognosis and the current escalating situation action plans must be adjusted and need to become tighter in future years. Transportation emissions of 8220 Mt of CO_2 have been reported, which are equivalent of 24.5 % of emissions worldwide, in 2019 [2]. The transportation sector is one of the largest CO_2 emitters, but also one of the hardest sectors to decarbonize, due to the necessity of fuel for combustion engines. One way of reducing emissions are renewable transportation fuels like hydrogen. Hydrogen is especially beneficial for the transportation sector because it is the only fuel, which produces zero emissions during the combustion process. Internal combustion engines utilizing hydrogen as fuel can reduce the necessity and dependency on the oil and gas industry for fossil fuel, as well as on critical raw materials like Lithium and Cobalt, for electric vehicle batteries. This thesis is in line and especially relevant for the growing hydrogen economy and further development.

1.2 Research Topic & Research Questions

The topic of the present work is the Flame Propagation of Hydrogen Combustion. Optical studies with high-speed schlieren imaging in a constant volume chamber as well as 1D simulations with Cantera is aiming to characterize the flame propagation of hydrogen. The following research questions have been established and are guiding through the research:

- Question 1) How to measure the hydrogen combustion flame front propagation with schlieren method in a constant volume combustion bomb?
- Question 2) How do various parameters, like initial temperature, pressure, dilution, and relative air-to-fuel ratio (λ) or equivalence ratio (ϕ) affect the flame speed?
- Question 3) How do the measurements compare with laminar flame speed computations?

The outline of this thesis are the literature review in Section 2 including hydrogen properties, combustion theory (laminar and turbulent flames), hydrogen engines and fuel cells, hydrogen production and safety. Section 3 deals with the Cantera combustion simulation, including theory and results. The next section, Section 4 presents the experimental setup, the validation matrix, the schlieren imaging, and the post-processing. Lastly, Section 6 is combining analysing and discussing the experimental work, and compares in the end simulations and experiments. Conclusions are drawn in Section 6.

2 Hydrogen

The following section is treating hydrogen, the fuel used within the simulations and experiments throughout this thesis. It also describes the fuel properties in comparison with other gaseous fuels like ammonia (NH_3) and methane (CH_4). Further, the general suitability of hydrogen as a fuel, hydrogen used in different kind of internal combustion engines, hydrogen production, safety aspects and concerns are covered.

2.1 Properties

The main properties of H_2, CH_4 and NH_3 are summarized in Table 1. The values are given for a temperature of 300 K and pressure of 1 atm.

Property:	**H_2**	**CH_4**	**NH_3**
Molecular Weight [g/mol]:	2.016	16.043	17.031
Density [kg/m^3] :	0.08	0.65	0.68
Mass Diffusivity in air [cm$^2/s$] :	0.61	0.16	0.228
Minimum Ignition Energy [mJ]:	0.02	0.28	8
Minimum Quenching Distance [mm]:	0.64	2.03	6.985
Flammability limits in air [%vol]:	4 - 75	5 – 15	15 - 28
Flammability limits:	$\lambda : 10 - 0.14$; $\phi : 0.1 - 7.1$	$\lambda : 2 - 0.6$; $\phi : 0.5 - 1.67$	$\lambda : 2.5 - 0.7$; $\phi : 0.4 - 1.4$
Lower Heating Value [MJ/kg]:	120	50	18.5
Higher Heating Value [MJ/kg]:	142	55.5	22.5
Stoichiometric air-fuel ratio [kg/kg]:	34.2	17.1	6.06

Table 1: Fuel Properties [3][4][5]

In brief, hydrogen is a small and light gas compared to CH_4 and NH_3, with low density under atmospheric conditions. It is a very mobile / diffusive gas, as shown by the high mass diffusivity number. Further, it has a low minimum ignition energy and a very wide range of flammability limits in contrast to the other fuels. These properties allow big ranges of equivalence ratios and therefore, a big range of engine power output. The range can be extended through increasing temperature and decreasing pressure. The difference between lower and higher heating value is explained through the condensation heat release of water, the single product of hydrogen combustion.

2.2 Combustion Theory

In this section the combustion theory is studied, in particular the basic flame terminology and flame theory, with a focus on laminar and turbulent flame propagation.

2.2.1 Flame Terminology

The process of combustion is set to stoichiometric conditions, which means the fuel and the oxidizer consume each other completely. In other words, the combustion is complete, without excess air or fuel and the products are only CO_2 and water (H_2O).

Stoichiometric reaction of hydrogen (fuel) and oxygen (oxidizer):

$$2\ H_2 + O_2 \rightarrow 2\ H_2O \tag{1}$$

Rich (excess fuel) reaction of hydrogen (fuel) and oxygen (oxidizer):

$$3\ H_2 + O_2 \rightarrow 2\ H_2O + H_2 \tag{2}$$

Lean (excess oxygen) reaction of hydrogen (fuel) and oxygen (oxidizer):

$$2\ H_2 + 2\ O_2 \rightarrow 2\ H_2O + O_2 \tag{3}$$

In a reaction, the reactants are located on the left and the products on the right. Each element consists of one mole, if not stated otherwise. The mole fraction of the stoichiometric fuel and oxygen mixture is calculated as followed, ν describing the mole number of O_2 [6]:

$$x_{fuel,stoich} = \frac{1}{1+\nu} \tag{4}$$

It is important to denote, that if air is used as oxidizer, the mixture contains of 21 % of oxygen, 78 % of nitrogen and 1 % of nobel gases, which equals to $x_{N_2} = 3.762\ x_{O_2,stoich} = \nu\ x_{fuel,stoich}$. The air equivalence ratio λ is the inverse of the fuel equivalence ratio $\phi = \frac{1}{\lambda}$, which are both used to describe if a reaction is lean, stoichiometric or rich. The air equivalence ratio is defined as following [6]:

$$\lambda = \frac{(\frac{x_{air}}{x_{fuel}})}{(\frac{x_{air,stoich}}{x_{fuel,stoich}})} \tag{5}$$

where x_i describes the mole fraction of the different reactants. As explained previously, rich combustion has excess fuel, which means $\phi > 1, \lambda < 1$. Stoichiometric conditions have $\phi = 1, \lambda = 1$ and lean combustion, with excess air, has values for $\phi < 1, \lambda > 1$.

2.2.2 Flame Theory

The combustion process can be divided into two different categories, premixed and non-premixed fuel-air mixtures. Each category on the other hand can be separated into laminar and turbulent flames.

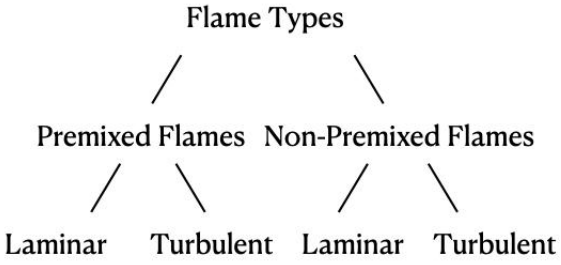

Figure 1: Flame Types [6]

Premixed flames include flames, where the fuel and oxidizer, most commonly air, is mixed before it is burned. Non-premixed gas mixtures, are not mixed prior to the combustion. Due to the higher relevance of the premixed type and the selection of the combustion process, the focus is on premixed laminar flames in this thesis. The flame speed represents the movement of the unburned gas, in the direction normal to the wave surface, through the combustion wave. It constitutes the main parameter studied in this thesis.

2.2.3 Laminar Flames

Laminar flames are described with the following governing equations, mass conservation (continuity), momentum conservation, species conservation and energy conservation.

Mass conservation [6][7][8]:

$$\frac{\partial \rho}{\partial t} + \nabla \cdot (\rho \vec{v}) = 0 \tag{6}$$

where ρ represents the density, t the time and $\vec{v}$ the velocity. The ideal gas law is considered to be valid and used to gain the density. The equation states that the mass entering and leaving the system is equal.

Momentum conservation [6][7][8]:

$$\frac{\partial (\rho \vec{v})}{\partial t} + \nabla \cdot (\rho \vec{v} \vec{v}) = \nabla p + \nabla \cdot \tau \tag{7}$$

where ρ represents the constant density. A incompressible flow is assumed. t describes the time, $\vec{v}$ the velocity and τ the viscous stress. Further, $\nabla \cdot (\rho \vec{v} \vec{v})$ describes the convection and $\nabla \cdot \tau$ the diffusion term. It states that the total momentum remains constant in the system.

Species conservation [6][7][8]:

$$\frac{\partial(\rho Y_i)}{\partial t} + \nabla \cdot (\rho Y_i \vec{v}) = \nabla \cdot (\rho \tilde{D} \nabla Y_i) + \omega_i \tag{8}$$

where $\nabla \cdot (\rho Y_i \vec{v})$ represents the convection term, Y_i is the mass fraction of the species i, $\nabla \cdot (\rho \tilde{D} \nabla Y_i)$ the diffusion term, $\tilde{D}$ represents the unity Lewis number for all species, and ω the chemical reaction rate. The species conservation equation shows the species mass, which is transported and transformed. It highlights the mass change of species due to diffusion, macroscopical flow and chemical reactions.

Energy conservation [6][7][8]:

$$\frac{\partial(\rho h)}{\partial t} - \frac{\partial p}{\partial t} + \frac{\partial(\rho \vec{v} h)}{\partial x} = \nabla \cdot (\rho \alpha \nabla h) + \dot{Q}_r + \tau : \nabla \vec{v} \tag{9}$$

The energy conservation describes the internal energy or enthalpy results from potential, kinetic and total energy. Where ρ is the density, p the pressure, t the time, $\vec{v}$ the velocity, h is the enthalpy, α the thermal diffusivity, τ the viscous stress, $\rho \alpha \nabla h$ the heat flux and $\dot{Q}_r$ the heat release.

In this thesis, only 1D premixed laminar flames are considered. It can be assumed that the flames are steady state, one dimensional, planar, stretch-free, adiabatic, with steady flow conditions, low Mach numbers and unity Lewis number. The kinetic and potential energies, viscous shear work, and thermal radiation is assumed to be negligible. The flame is considered to have constant pressure and binary diffusion. This results into a flame velocity of [6][7]:

$$v_L = \sqrt{\frac{\alpha}{\tau}} \tag{10}$$

where $\tau = \frac{1}{k} = [A\ exp(-E/RT)]^{-1}$ for $T < T_b$ (burned gas Temperature). The velocity depends only on the diffusivity and the time of reaction.

2.2.4 Turbulent Flames

Turbulent flames are mostly unstudied and are very complicated. Turbulent flows are unsteady, with continuous velocity fluctuations, which lead to density, temperature and mixture fluctuations. These fluctuations are generated by shear within the flow. The speed is continuously changing in speed and direction. High Reynolds numbers are an indicator for turbulent flows. The Reynolds number is defined as [6]:

$$Re = \frac{\rho v l}{\mu} \tag{11}$$

where l describes the length of the system, ρ the density, v the velocity and μ the viscosity of the fluid.

Generally, turbulent flames are high speed flames compared to the smooth burning laminar flames, which are categorized as low speed flames. The turbulent flame speed is defined as [6]:

$$v_T = v_L(1 + \frac{v}{v_L}) = \frac{v_L A_L}{A_T} \tag{12}$$

where v denotes the root mean square velocity of the fluctuations, A_L the laminar flame area and A_T the turbulent flame area. This type of flames is out of the scope of this thesis, it is mentioned for completeness and it will be considered for future studies.

2.3 Hydrogen Internal Combustion Engines

The first attempt to develop hydrogen engines was in 1820 by Reverend W. Cecil. Generally, converting an internal combustion engine to run on hydrogen is not very difficult, but to gain good efficiencies and maintain well running behaviour is the major issue of hydrogen internal combustion engines. The first reported attempt to use gas as fuel was in the 1860s to 1870s by Nikolaus A. Otto, where a synthetic gas with a hydrogen content over 50 % was utilized. In recent years, the interest of carbon and pollution free vehicles and independence of the oil industry has returned [9].

Currently, not many cars contain of hydrogen internal combustion engines, this is expected to change in the near future. Properties in favor of hydrogen combustion are high thermal and mass diffusivity, which helps to achieve homogeneity inside the combustion chamber. Additionally, low minimum ignition energy and wide flammability limits support a stable combustion through a wider range of fuel-air mixtures, including the ability to combust on lean conditions, which decreases nitrogen oxides (NO_x) emissions and increases complete combustion. Moreover, hydrogen has a relatively high auto-ignition temperature, which allows higher compression ratios in the engine, which is positively reflecting on the thermal efficiency of the system. Hydrogen has very high flame speeds at stoichiometric conditions, which allows to operate closer to thermochemically ideal engine cycles. Lastly, the small quenching distance allows better combustion efficiency [9].

On the other hand, low ignition energies can create problems with premature ignition and flashback. The small quenching distance also increases the probability of backfiring due to the flames being closer to the cylinder wall. The high auto-ignition temperature also increases the difficulty to ignite the fuel inside diesel engines due to the necessity of high temperatures to ignite hydrogen. Furthermore, hydrogen has a very low density, for which it requires large volumes of hydrogen storage capacity and the additional low energy density, which reduces the power output [9].

Internal combustion engines can be categorized by their fuel injection method into either port fuel injection or into direct injection, see Figure 2. The difference between the two methods is, that port fuel injection usually utilizes a spark discharge to ignite the fuel, while direct injection utilizes spark-assisted or hot-surface-assisted ignition. In a second stage, the engines can be divided after their ignition strategy [10].

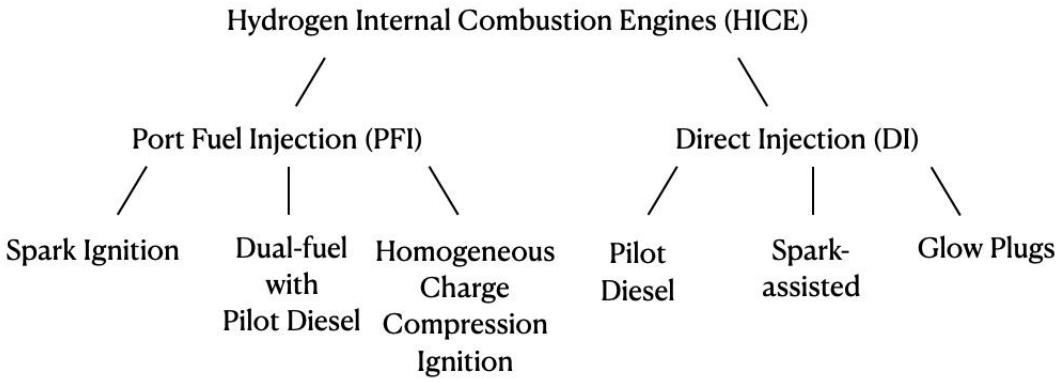

Figure 2: Categorization of Hydrogen Internal Combustion Engines [10]

2.3.1 Port Fuel Injection

Port fuel injection strategy describes the strategy where the fuel is injected into a intake port upstream or a pre-combustion chamber during the intake stroke to mix with the incoming air before entering the combustion chamber. Disadvantages of port fuel injection strategy are pre-ignition, knocking and backfiring, caused by the low minimum ignition energy and small quenching distance of hydrogen. The power output and efficiency for the port fuel injection method is reduced due to engine power density limitations of displaced air in the intake and increased work for the compression stroke [9][10]. Forms of engines utilizing port fuel injection method are homogeneous charge compression ignition, spark ignition and pilot diesel engines.

Spark ignition engines widely utilize port fuel injection strategy. These spark-ignited engines can run at ultra-lean conditions to achieve very low NO_x emission levels without after-treatment and overcome the challenges knocking, pre-ignition and backfiring. Lean conditions also increase the minimum ignition energy, reduce heat losses and increases the charge specific heat ratio, but it also limits the engine power output [10].

Dual-fuel engines, which use hydrogen port fuel injection strategy in combination with a pilot diesel fuel is a promising strategy to overcome the drawbacks of pure diesel and hydrogen engines. The flexibility of total energy input of this engine type through the hydrogen share is a major advantage. The excessive pressure rise during hydrogen combustion increases the probability of knocking and pre-ignition, which limits the hydrogen energy share of about 30 - 40 % for low and medium loads, and 6 - 25 % for high loads. However, studies have been made till 97 % hydrogen share. Unfortunately, with increasing hydrogen share the engine efficiency is decreasing. Additionally the NO_x emissions are increasing and other emissions like CO, PM and CO_2 are exhausted [10].

Homogeneous charge compression ignition engines can form homogeneous hydrogen-air mixture, which makes very fuel-lean combustion possible. These conditions support lowering NO_x formation, close to zero, while providing high engine efficiencies. The utility of low-temperature combustion mode is limited due to the high auto-ignition temperature and therefore, high compression ratios, of hydrogen. Additional challenges are the control of phasing and peak pressure rises, as well as, the engine reliability due to high amounts of heat release. However, only limited loads can be achieved with homogeneous charge compression ignition engines [10].

2.3.2 Direct Injection

Direct injection is the injection strategy to inject the fuel directly into the cylinder during the compression stroke (intake valve closed). It is an attempt to improve the engine performance and avoid / reduce the risk of backfiring and pre-ignition. Also the volumetric efficiency loss through displacement of air can be avoided. Dependent on the injection time, high injection pressure (over 100 bar) might be required, which again increases the fuel mass flow rate and therefore, the energy input. Several parameters have an effect on the operation of the high pressure direct injection operation, these parameters are injection pressure, injection duration, injection orientation and ignition timing. Under optimal conditions, similar efficiencies like diesel engines can be achieved. The high auto-ignition temperature of hydrogen is still an issue which has to be overcome [9][10].

Spark-assisted hydrogen direct injection and glow plugs operate similarly, with glow plugs replaced by spark plugs. The spark / glow plugs are utilized to assist the cold start of an engine by electrically heating the surface surrounding the combustion chamber. The injection timing was found to be the biggest influencing media of the engine performance and emissions. The compression work can be reduced by injecting the fuel into the chamber at the compression stroke. For low and medium load, when a less homogeneous mixture (delayed injection timing) is combusted, higher NO_x emissions are expected. For high loads early injection favors high NO_x emissions. Next to the geometry and operating conditions, also the injection angle has a significant impact on the engine performance [10].

For hydrogen internal combustion engines the glow plug has to work continuously to ensure hydrogen ignition in every engine cycle. The temperature range of the glow plug is from 1200 - 1400 K. Glow plugs are a reliable ignition source for hydrogen internal combustion engines, but the fuel consumption is increasing through their use. Especially for high loads, large amounts of NO_x emissions are exhausted. The reliability and durability of the glow plug is questionable due to the high surface temperatures, this is why the technology is rarely used [10].

2.3.3 Other Strategies

In recent years a dual injection strategy has been developed. This strategy combines direct injection and port fuel injection injection to gain the benefits of both injection strategies. Other strategies to diminish some of the hydrogen combustion problems are exhaust gas recirculation or water injection. Exhaust gas recirculation is described as a recirculation of portions of the exhaust gases into the intake port of the engine. The recirculated gases reduce the hot spot temperature and therefore, the possibility of pre-ignition. An additional benefit of exhaust gas recirculation are reduced NO_x emissions due to reduced peak combustion temperatures. On the contrary, the engine power output is reduced, caused by reduced fuel share during the combustion. A percentage of 25 - 30 % recirculation prevents backfiring. Other ways aiding to control effects like pre-ignition and knocking is to re-design the combustion chamber and cooling system for hydrogen use [9].

2.4 Hydrogen Fuel Cells

Most commonly proton exchange membrane fuel cell are used in today's fuel cells utilized in forklifts or other small scale vehicles. Proton exchange membrane fuel cell has the ability of low-temperature operation, it has a good performance and a fast response time, these are the reasons for proton exchange membrane fuel cell preference in vehicles [11].

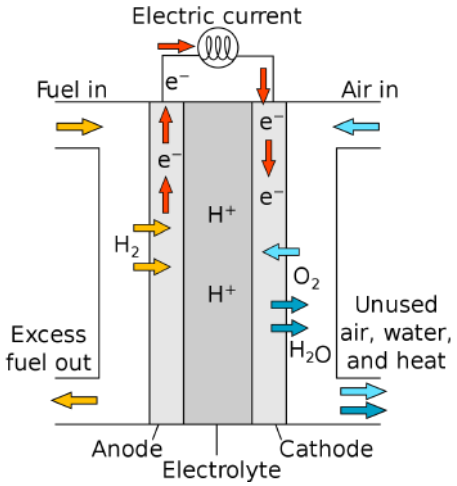

Figure 3: Fuel Cell Representation taken from PEM Fuel Cell Dataset [12]

A fuel cell consists of an anode, a cathode and an electrolyte located between anode and cathode (Figure 3). Pure hydrogen is fed into the anode side, where electrons are separated by the membrane, while moving towards the cathode side. Hydrogen ions and air pass through the membrane, combining to H_2O.

2.5 Comparison of Hydrogen Internal Combustion Engines with Fuel Cell Electric Vehicles

Combining proton exchange membrane fuel cells with an electric vehicle a hybrid fuel cell electric vehicle competitive to battery electric and fossil fuel vehicle is emerged. In this occasion the fuel cell is used as the driving force, just like a internal combustion engine of a conventional vehicle [13]. Fuel cell electric vehicles have higher efficiencies, lower emissions, a good cold-start capabilities and they operate without generating vibration and noise [14]. The main problem with fuel cell electric vehicles is the hydrogen's low energy density, and therefore arising weight issues, which have to be reduced drastically to be competitive to hydrogen internal combustion engines. Large storage tanks increase the weight, which are necessary to be able to store enough hydrogen on-board [15]. A secondary challenge is the need for critical raw materials like platinum or cobalt. A major role for the decision for or against hydrogen internal combustion engines or fuel cell electric vehicle plays the overall cost of the vehicles. hydrogen internal combustion engines have essentially lower capital expenditure and infrastructural costs than fuel cell electric vehicles, while the fuel costs are of a similar price range, but the maintenance costs are much higher for hydrogen internal combustion engines than for fuel cell electric vehicles. The range, the refuelling speed and the lifetime of the vehicles are about the same [16].

2.6 Production

Till today hydrogen is mostly produced from fossil fuel like natural gas or oil. Hereby, hydrogen is produced as a by-product of the chemical processes. Other more sustainable ways, of hydrogen production, is by electrolysis or gasification. Hydrogen production has the requirement of a simple process, easy to get, low cost and environmentally safe [17]. The production of hydrogen have several color codes dependent on their primary energy source for the hydrogen production process.

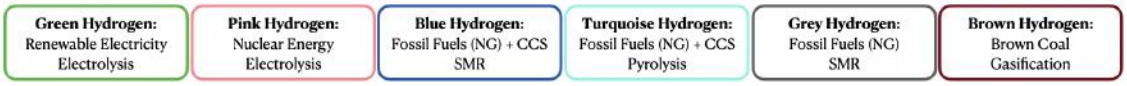

Figure 4: Overview of the Production Paths of Hydrogen

Grey Hydrogen: Is the most common way of producing hydrogen. The hydrogen is produced by steam methane reformation of fossil fuels. This process produces CO_2, which is not captured but emitted to the atmosphere [18].

Blue Hydrogen: Is hydrogen produced by steam methane reformation of fossil fuels, including a carbon capture and storage process, where CO_2 is stored underground. The CO_2 is not fully emitted to the atmosphere and therefore, considered as path towards green hydrogen and carbon neutrality [18].

Green Hydrogen: Is the most sustainable form of hydrogen. It is produced through water electrolysis, decomposition of water into its components hydrogen and oxygen, energized by renewable electricity. No CO_2 is generated during this production process [18].

Black / Brown Hydrogen: It is hydrogen produced from bituminous (black) or lignite (brown) coal. The color of the coal is referring to the color type of the hydrogen produced. The coal is gasified, producing large amounts of CO_2 and CO, which is released into the atmosphere [19].

Purple / Pink Hydrogen: Purple and pink hydrogen is called hydrogen produced through nuclear power [18][19].

Turquoise Hydrogen: Hydrogen produced by methane pyrolysis is called turquoise hydrogen. The CO_2 is captured in a solid form, instead of gaseous. This process is still not fully matured [18].

White Hydrogen: Is geological occurring from underground deposits resulted through fracking. Currently, it is not possible to exploit white hydrogen [19].

In the future, with increasing hydrogen demand, more color codes and more hydrogen production processes will occur, like yellow hydrogen, hydrogen from solar energy.

2.7 Safety Aspects & Concerns

Especially the wide flammability limits, low minimum ignition energy of hydrogen and high burning velocity are raising public concerns. Also dramatic incidents in the past, like Fukushima, soil the image of hydrogen. The storage of hydrogen is due to its low volumetric density and the safety of the storage system rather difficult. Other challenging aspects of hydrogen are that hydrogen is colourless, odourless, and tasteless, which cannot be detected by human senses. A study shows that hydrogen can be divided into the following risk categories [14]:

- Hydrogen dispersion and explosion
- Hydrogen leakage diffusion
- Hydrogen embrittlement
- Thermal radiation
- Hydrogen jet fire
- Hydrogen ignition
- High-pressure hydrogen leakage
- Cryogenic hydrogen releases

The main outcome of the risk analysis is that, up to 15 % hydrogen concentration in confined spaces is acceptable, an increase of alloy strength and hydrogen pressure increases hydrogen embrittlement, and if the initial pressure of released hydrogen is low, no spontaneous combustion is expected [14].

Hydrogen embrittlement is a phenomenon which happens if metals are exposed to hydrogen, leading to degradation of the metals' mechanical properties, failure, and leaks. It needs to be considered, when resulting in cracking, emerging through sufficient stress on objects like hydrogen storage systems or transmission pipelines. The material purity, surface conditions, exposure time and environmental pressure and temperature have an effect. The higher hydrogen purity, the higher the vulnerability of steel to embrittlement. Moreover, in a high-pressure hydrogen gas environment increasing alloy strength and hydrogen pressure results in increased hydrogen embrittlement [14].

3 Simulations

In this section all important aspects of the chemical kinetic simulations in Cantera are stated. The first subsection is about Cantera itself, the used mechanisms, and equations used inside the software. After that the simulation parameters are determined and results analysed and discussed.

3.1 Cantera - Theory

The simulations included in this thesis are carried out with the open-source, object-oriented software Cantera, Version 2.5.1. The software is integrated as a software extension package in a python interface. It is used to solve premixed hydrogen combustion 1D-laminar flame propagation calculations inside a constant volume chamber, including chemical kinetics, thermodynamics and transport problems.

In the following paragraphs the calculations and equations utilized by Cantera are presented. Cantera assumes all gases to be ideal gases, which means atoms are perfectly elastic and kinetic energy is the only form of internal energy. This results in the validity of the ideal gas law [20] :

$$pV = nRT \tag{13}$$

where P describes the absolute pressure, V the volume, n the number of moles, R the universal gas constant $R = 8.3145\ J/molK$ and T the absolute Temperature.

There are two transport models integrated in Cantera, the multicomponent and the mixture-averaged model. The difference between the two models is the accuracy of the solution of the Boltzmann equation, where the multicomponent model is the more exact one. The Boltzmann equation is described as [7]:

$$\frac{\partial f_i}{\partial t} + \frac{1}{m_i}(p \times \frac{\partial f_i}{\partial r}) + (F_i \times \frac{\partial f_i}{\partial p}) = \Sigma[\Gamma_{ij}^{(+)} - \Gamma_{ij}^{(-)}] \tag{14}$$

In the mixture-averaged transport model, the diffusion velocity for each gas is approximated in relation to the other gases' velocities approximation. This means, only one diffusion term D' is calculated [7]:

$$D' = \frac{1 - Y_i}{\sum_{j \neq i} X_j / D_{ji}} \tag{15}$$

Also the simulations with multi-averaged transport model assume zero thermal diffusion. The effects and differences between the transport models are studied in the thesis of Martin Torstensson [7]. He states, that the multi-averaged transport model is not varying much from the multicomponent transport model for hydrogen combustion. Based on the study, which highlights the qualification of the mixture-average model and to shorten computational and simulation times, the mixture-averaged model has been selected for this thesis.

In Cantera the diffusive fluxes are calculated as followed [21]:

$$j_k^* = -\rho \frac{W_k}{\overline{W}} D'_{km} \frac{\partial X_k}{\partial z} \tag{16}$$

and:

$$j_k = j_k^* - Y_k \sum_i j_i^* \tag{17}$$

where $\overline{W}$ represents the mean molecular weight of the mixture, D'_{km} the mixture-averaged diffusion coefficient and X the mole fraction. The second equation is the correction factor to ensure that the sum of the mass fluxes are zero, which it does not account for in the mixed-averaged model.

The flame model chosen is a freely propagating premixed flat laminar flame. Cantera uses axisymmetric stagnation flow to reduce the three-dimensional governing equations to one-dimensional. The tangential velocity is assumed to be zero. The Governing equations are deposited as following [21]:

Continuity:

$$\frac{\partial \rho u}{\partial z} + 2\rho V = 0 \tag{18}$$

Radial momentum:

$$\rho u \frac{\partial V}{\partial z} + \rho V^2 = -\Lambda + \frac{\partial}{\partial z}(\mu \frac{\partial V}{\partial z}) \tag{19}$$

Energy:

$$\rho c_p u \frac{\partial T}{\partial z} = \frac{\partial}{\partial z}(\lambda \frac{\partial T}{\partial z}) - \sum_k j_k c_{p,k} \frac{\partial T}{\partial z} - \sum_k h_k W_k \dot{\omega}_k \tag{20}$$

Species:

$$\rho u \frac{\partial Y_k}{\partial z} = -\frac{\partial j_k}{\partial z} + W_k \dot{\omega}_k \tag{21}$$

where ρ describes the density, u the axial velocity, v the radial velocity, $V = v/r$ the scaled radial velocity, Λ the pressure eigenvalue, μ the dynamic viscosity, c_p the heat capacity (constant pressure), T the temperature, λ the thermal conductivity, Y the mass fraction, j the diffusive mass flux, h the enthalpy, W the molecular weight and $\dot{\omega}$ the molar production rate.

Inlet boundary conditions for temperature T_0, pressure P_0, mass Y_0/ mole X_0 fraction of fuel and oxidizer have to be entered in the beginning of the Cantera program. All necessary values are calculated to gain the scaled radial velocity v_0, the mass flow rate $\dot{m}_0$ is an eigenvalue which is determined while solving the equations. For a premixed laminar flat flame (freely propagating flames) the constraints are solving the energy balance and ensuring that the calculated temperature matches the entered one.

Equations used in Cantera are [21][22]:

$$T(z_0) = T_0 \tag{22}$$

$$V(z_0) = V_0 \tag{23}$$

$$\dot{m_0} Y_{k,0} - j_k(z_0) - \rho(z_0) u(z_0) Y_k(z_0) = 0 \tag{24}$$

$$\Lambda(z_0) = 0 \tag{25}$$

$$\epsilon_k = Y_k + \frac{j_{k,z}}{\dot{m_0''}} \tag{26}$$

$$v_L = \dot{m_0''}/\rho \tag{27}$$

where $\dot{m_0''}$ is the mass flux, ϵ the mass flux fraction of the unburned gas, Y the mass fraction and v_L the laminar burning velocity.

3.2 Mechanism Validation

To choose the optimal mechanism for the Cantera simulations, some validation simulations have been carried out. The experimental data for the validation was taken from the research papers of Pareja (2010) [23], Han (2019) [24], and Frassoldati (2006) [25].

Pareja et al. provides a experimental and numerical study on laminar burning velocities of NH_3/Air mixtures. They were performed at atmospheric pressure (1 atm), room temperature (293 K) and varying equivalence ratio from 0.8 to 3.0. The flames were generated by a contoured slot-type nozzle burner (4x10 mm). The measurements were done using particle tracking velocimetry combined with Schlieren photography [23]. Han et al. measures the laminar burning velocity of NH_3/N_2O/Air flames with the heat flux burner method at atmospheric pressure, room temperature (298 K), with varying equivalence ratios and N_2O mixing ratios [24]. Frassoldati et al. shows a comparison between the measurements and model results of a freely propagating H_2/N_2O flame. The experimental data given are a wide range of data related to NO_x formation in H_2 flames, but also laminar flame speeds, shock tube ignition delays, flow and stirred reactors.

The mechanisms chosen for the mechanism validation are taken from the study of Olm (2014) [26] about recent hydrogen mechanisms. Only mechanisms including the formation of NO_x emissions have been considered. Selected mechanisms are GRI-MECH 3.0 (1999) [27], CRECK (2003) [28], Wang (2019) [29], NUI Syngas/NO_x (2017) [30], San Diego (2011) [31] and Konnov (2019) [32]. The last two mechanisms are modified with an extension of the species species N, O and H and their correlating reactions. With the San Diego NO_x mechanism for San Diego and the mechanism of Capriolo (2021) [33] for Konnov.

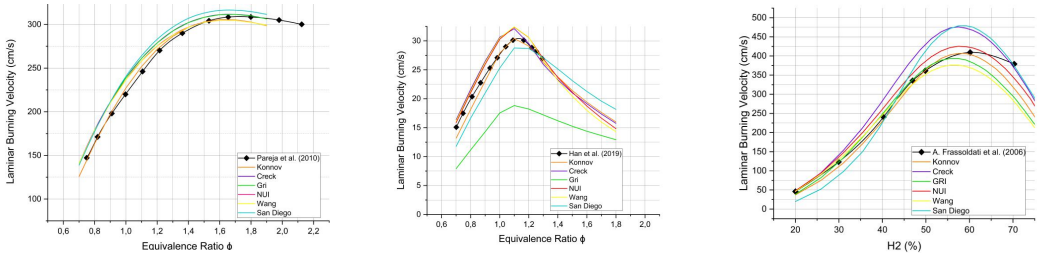

(a) (b) (c)

Figure 5: Cantera Mechanism Validation Comparison: a) H_2 + Air Combustion: T = 293 K, P = 1 atm, ϕ = 0.7 - 1.9; b) H_2 + NH_3 + Air Combustion: Fuel: 40 % H_2, 60 % NH_3, T = 298 K, P = 1 atm, ϕ = 0.7 - 1.3; c) H_2 + N_2O Combustion: T = 333 K, P = 0.09 atm, ϕ = 0.25 - 4. An expanded version of these graphs can be found in the Appendix A1, A2 and A3.

After the simulations are processed, the results in Figure 5 show that the hydrogen mechanism from Konnov including the NO_x mechanism has the best overall results for all three validation scenarios, single-fuel hydrogen combustion (Figure: 5 a), but also for dual-fual H_2 + NH_3 (Figure: 5 b), as well as the imaging of NO_x emissions (Figure: 5 c) are captured best with the mechanism from Konnov. Further analysis is only made with the selected mechanism of Konnov.

3.3 Simulation Parameters

The reference conditions for the simulations have been manifested to the following, Temperature of 300 K, Pressure of 5 atm, Equivalence ratio of 1.0, Dilution of 0 %, with an air (N_2: 3.76, O_2: 1.0) and fuel (H_2: 1.0) mixture. The flame structure for reference conditions has been analysed. Important hereby are H_2, O_2, hydroxide (OH) mole fractions, the temperature and NO emissions in parts-per-million (ppm) over the height of the burner flame. The simulations are carried out under the following conditions:

Variables	**Value 1**	**Value 2**	**Value 3**	**Value 4**	**Value 5**
Fuel Composition:	Air + H2				
Temperature:	300 K	500 K	1000 K		
Pressure:	2 atm	5 atm	10 atm	(20 atm)	(40 atm)
Equivalence Ratio:	0.4 - 2.5 in 0.1 steps				
Dilution:	0 %	10 %	20 %		

Table 2: Simulation Parameters

3.4 Simulation Results and Discussion

In the following subsection the simulation results gained with Cantera can be seen. First results obtained under reference conditions are presented. For each scenario the results are divided into four sub-graphs, a) H_2 mole fraction vs. temperature over the burner height (m) b) O_2 mole fraction vs. temperature over the burner height (m) c) OH radicals vs. temperature over the burner height (m) d) NO (ppm) vs. temperature over the burner height (m). After that, results for different parameter variations, as mentioned in Table 2, are displayed. The effects of equivalence ratio (Section: 3.4.2), initial chamber pressure (Section: 3.4.3), initial chamber temperature (Section: 3.4.4) and dilution (Section: 3.4.5) are examined and presented. More detailed analysis can be found in the Appendix A.

3.4.1 Simulations at Reference Conditions

Figure 6 shows the results of the simulations at reference conditions: T = 300 K, P = of 5 atm, $\phi = 1.0$ and Dilution = 0 %.

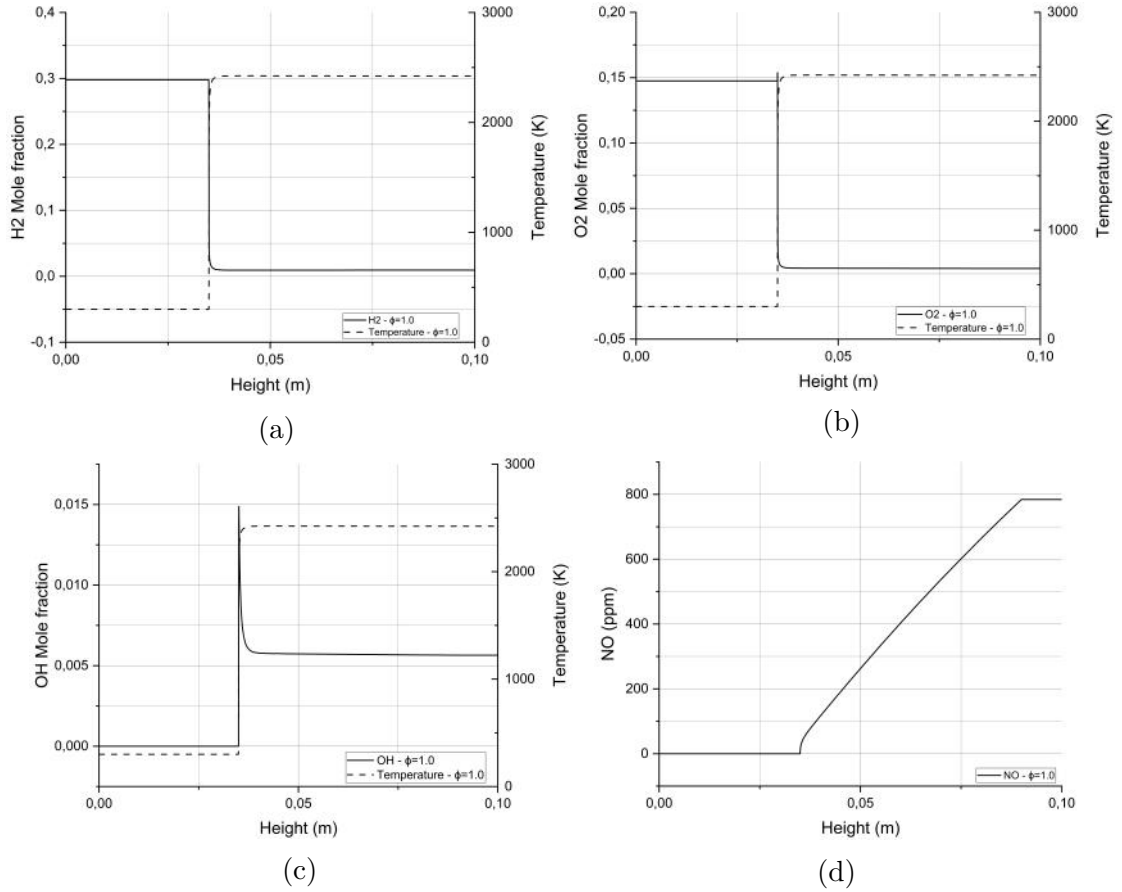

Figure 6: Reference Conditions: T = 300 K, P = 5 atm, $\phi = 1.0$, Dilution = 0 %: a) H_2 Mole Fraction vs. Temperature over the Burner Height; b) O_2 Mole Fraction vs. Temperature over the Burner Height; c) OH Radicals vs. Temperature over the Burner Height; d) NO (ppm) vs. Temperature over the Burner Height

The laminar burning velocity was found as 2.029 m/s for reference conditions. During the combustion process, the temperature is rising from the initial 300 K chamber temperature to as high as the maximum of 2424.1 K. With increasing temperature, the density is decreasing from 4.24 to just 0.613 kg/m^3. The fuel, H_2 and the oxidizer O_2 are converted within the process to H_2O. H_2 molecules decrease from 0.298 to 0.004 mole, while O_2 is decreasing from 0.147 to 0.0056 mole (Figure 6 and 0.33 mole of H_2O is produced a) b)). The OH radicals are increasing from 0 till 0.0149 mole, where the reaction is about to start and decrease to 0.006 mole, where the combustion process ends (Figure 6 c)). The OH radicals are consumed within chemical reactions of the combustion. Alongside H_2O, NO_x emissions in the form of 0.00078 mole or 784.4 ppm of NO is produced (Figure 6 d)).

3.4.2 Effect of the Equivalence Ratio

To get an insight into the effect of the equivalence ratio on the flame speed and the flame structure, the same simulations with reference conditions (T = 300 K, P = 5 atm, Dilution = 0 %) and an equivalence ratio of $\phi = 0.5$ have been carried out.

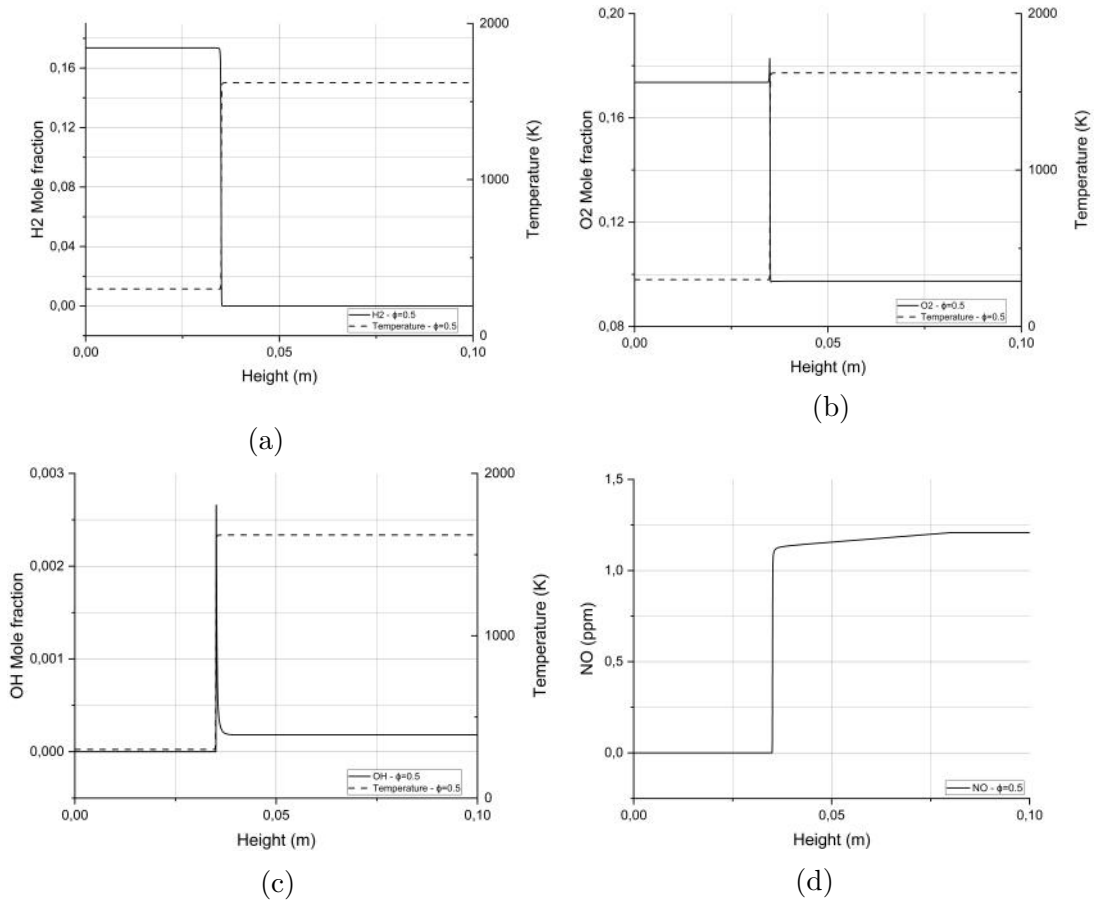

Figure 7: Equivalence Ratio Variation with Simulation Conditions: T = 300 K, P = 5 atm, $\phi = 0.5$, Dilution = 0 %: a) H_2 Mole Fraction vs. Temperature over the Burner Height; b) O_2 Mole Fraction vs. Temperature over the Burner Height; c) OH Radicals vs. Temperature over the Burner Height; d) NO (ppm) vs. Temperature over the Burner Height

The graphs show the decreased amount of H_2, increase amount of O_2 and therefore, decreased OH mole fraction. The lean combustion process not only reduces the combustion temperature to about 1621 K, it also decreases NO emissions, through the lower combustion temperature, to 1.2 ppm instead of 784.4 ppm in the $\phi = 1$ case. The lower combustion temperature caused by the lower H_2 content is decreasing the reactivity of the mixture (lower OH Radicals), which in turn decreases the laminar burning velocity to 0.22 m/s.

The following Figure 8 shows that the laminar burning velocity is changing over the equivalence ratio spectrum and also highlights the impact of different initial chamber pressures.

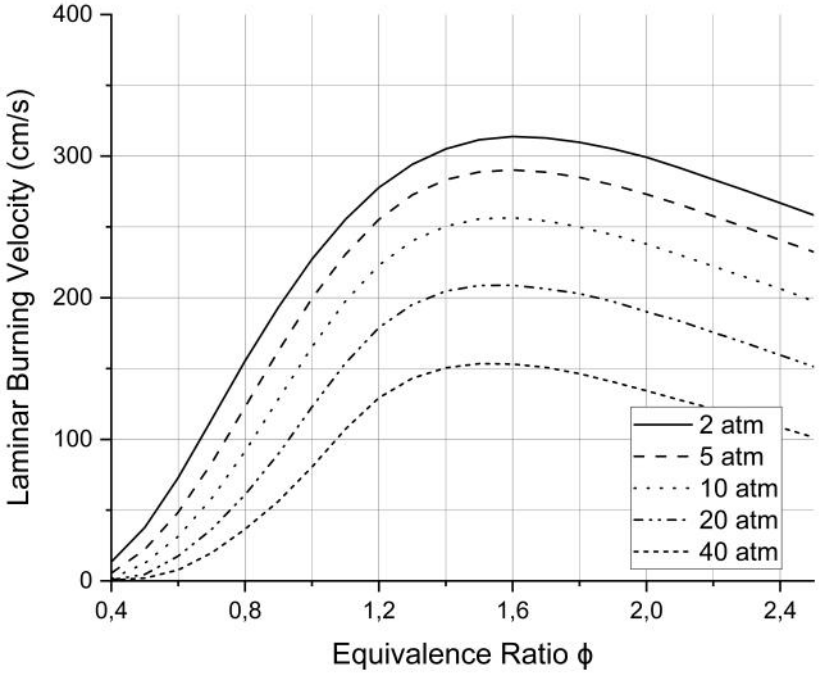

Figure 8: Equivalence Ratio vs. Laminar Burning Velocity: T = 300 K, P = as stated, ϕ = 0.4 - 2.5, Dilution = 0 %

The peak can be observed between an equivalence ratio of 1.5 - 1.6 dependent on the initial pressure. The graph shows higher laminar burning velocity for lower initial pressures. This phenomena can be explained through the increase in density, which decreases the laminar burning velocity, since the laminar burning velocity and the density are directly related (Equation 29) .

The shape of the graph can be explained by the interdependency of the laminar burning velocity with the adiabatic flame temperature (T_{ad}) and on the diffusivity of hydrogen. T_{ad} describes the maximum temperature for the given reactants in a combustion process. Dependent on the conditions (initial temperature, initial pressure, equivalence ratio) of the combustion, T_{ad} varies. The T_{ad} shows higher values, when higher amounts of heat are released through the combustion process. Higher heat releases also means higher flame speeds [34].

The Figure 9 is showing the T_{ad} for hydrogen at the reference conditions over the equivalence ratio. The curve reaches its peak T_{ad} at an equivalence ratio of 1.1 (rich combustion).

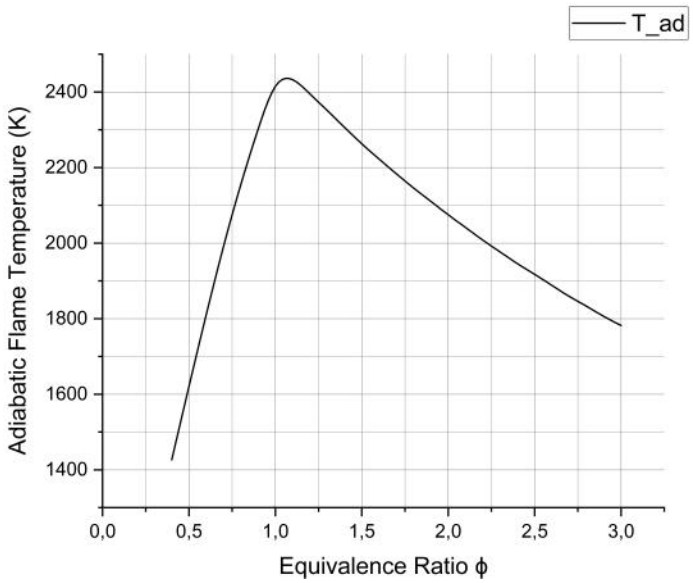

Figure 9: Equivalence Ratio vs. Adiabatic Flame Temperature: T = 300 K, P = 5 atm, ϕ = 0.4 - 3.0, Dilution = 0 %

In the case of hydrocarbon combustion the peak of the T_{ad} and the peak of the laminar burning velocity are very close together. For hydrogen combustion it is not the case, as shown in Figure 8 and Figure 9. The laminar burning velocity peaks around 1.6, while the T_{ad} peaks at an equivalence ratio of 1.1. This offset can be explained by the second interdependency of the laminar burning velocity of hydrogen, the high diffusivity of hydrogen. The following relations are relevant to understand the behaviour shown in Figure 8 [34]:

$$v_L \propto \sqrt{D\Omega} \tag{28}$$

$$v_L \propto \sqrt{\frac{\dot{Q}_r \alpha}{\rho c_p \triangle T}} \tag{29}$$

where D is the mass diffusivity and Ω the reaction rate, α the thermal diffusivity, c_p the specific heat ρ the density. The main parameters, which affect the flame speed are Ω, which is influenced by T_{ad}, as discussed above and $Le = \frac{\alpha}{D}$, which turns into $v_L \propto \sqrt{Le}$. The Le number for lean H_2-Air mixtures is around 0.33 and for rich around 2.3, this is the reason for the peak shift towards the richer side of the combustion process [34].

3.4.3 Effect of the Chamber Pressure

In this section the effect of the initial chamber pressure has been studied. Apart from the pressure, the reference conditions have been kept. Since for the comparison of simulations and experiments only 2 - 10 atm are relevant, only those are presented. In the Appendix A4, a more detailed version with 20 and 40 atm can be found.

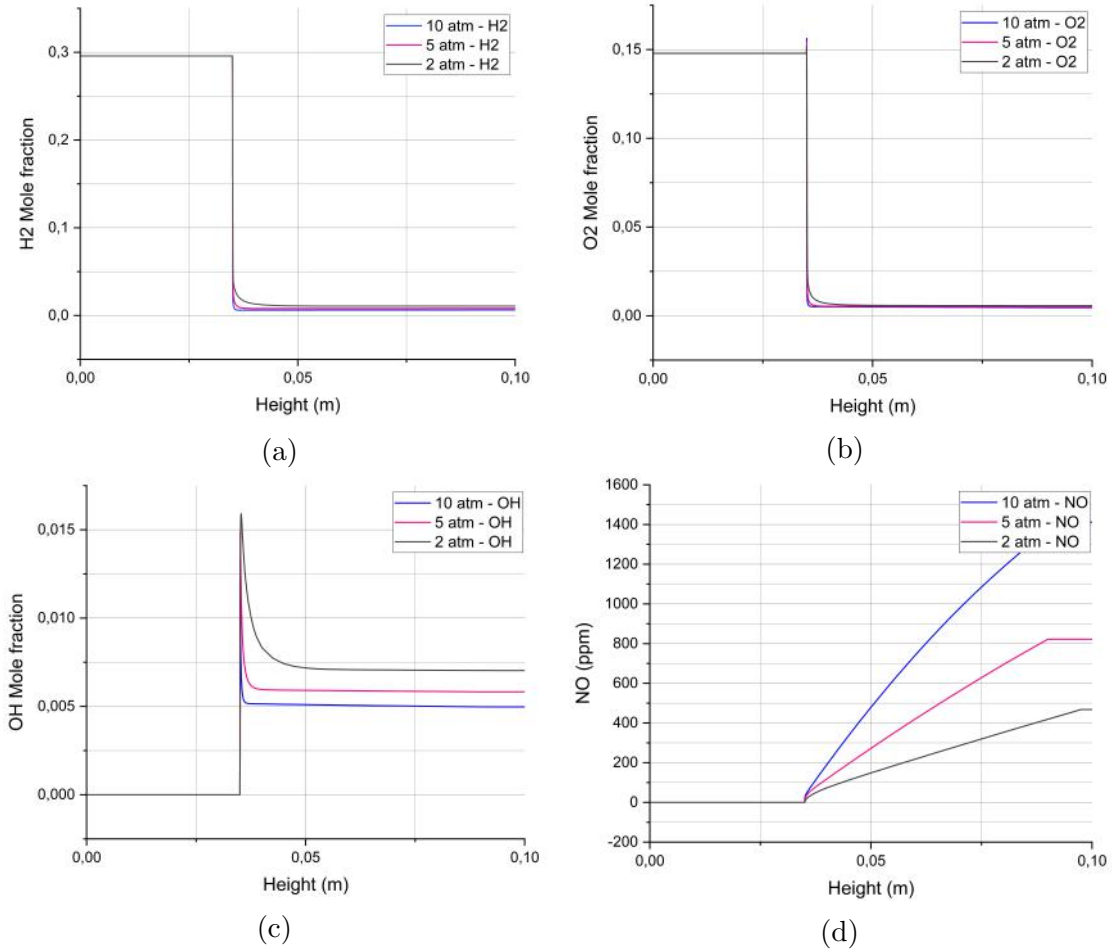

Figure 10: Pressure Effect: T = 300 K, P = as stated, $\phi = 1.0$, Dilution = 0 %: a) H_2 Mole Fraction vs. Burner Height; b) O_2 Mole Fraction vs. Burner Height; c) OH Radicals vs. Burner Height; d) NO (ppm) vs. Burner Height

The laminar burning velocity is decreasing for increasing pressure levels. For 2 atm a laminar burning velocity of 2.27 m/s, for 5 atm 2.029 m/s and for 10 atm 1.65 m/s are expected. It highlights that increasing the initial chamber pressure is slowing down the laminar burning velocity, which is based on the increasing density for higher pressures [34]. The combustion temperature is increasing in a similar way for all initial pressure levels. The H_2O production, the H_2 and the O_2 content stay fairly constant for all pressures considered (Figure 10 a) b)). The OH radicals left after the combustion process are decreasing for increasing pressure levels (Figure 10 c)).

It shows that NO emissions are increasing with increasing pressures (Figure 10 d)). This can be explained with the creation process of NO_x. The emissions are divided into prompt NO_x, which is created in the freely propagating laminar flame, close to chemical equilibrium, where the heat release has been mostly completed and the slow-forming postflame NO_x, which is created downstream of the instantaneous heat-release region. It was found, that the pressure is effecting the two NO_x types differently. While prompt NO_x is decreasing with increasing pressure, postflame NO_x is increasing. Moreover, it could be proven, that for high temperatures prompt NO_x is dominating, since in this case only temperatures of 300 K are considered, postflame NO_x is dominant, which is increasing the NO_x levels with increasing pressure [35].

3.4.4 Effect of the Mixture Temperature

Hereafter, the effect of the mixture temperature has been presented. More detailed graphs can be found in the Appendix A5 - A7.

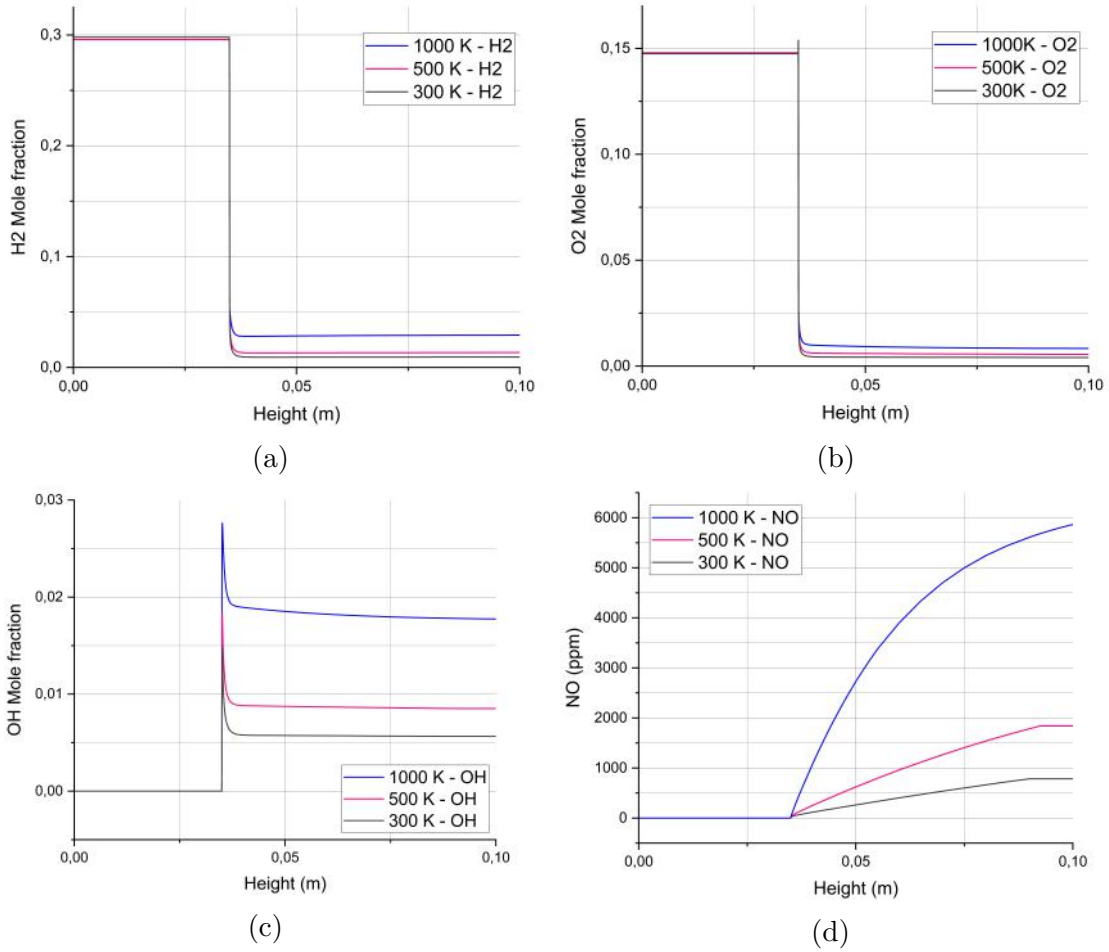

Figure 11: Temperature Effect: T = as stated, P = 5 atm, $\phi = 1.0$, Dilution = 0 %: a) H_2 Mole Fraction vs. Burner Height; b) O_2 Mole Fraction vs. Burner Height; c) OH Radicals vs. Burner Height; d) NO (ppm) vs. Burner Height

The laminar burning velocity is drastically increasing for increasing temperature levels to as high as 22.19 m/s for 1000 K. The final temperature of the combustion is rising, while the density is decreasing with increasing initial temperature. The higher the unburned gas temperature, the less H_2O is produced during, but the more H_2 is remaining after the combustion (Figure 11 a)). For higher temperatures less O_2 is consumed (Figure 11 b)). The OH radicals left after the combustion process are higher for 1000 K compared to 500 or 300 K (Figure 11 c)). The study shows that NO emissions are increasing from 300 to 1000 K, with a steeper increase for higher initial temperatures (Figure 11 d)). Postflame NO_x is highly dependent on the temperature. With increasing temperatures the NO_x levels are increasing, since in higher temperature environment the bond breakage of nitrogen (N_2) and O_2 is much simpler. The temperature effect is much stronger than the pressure effect [35].

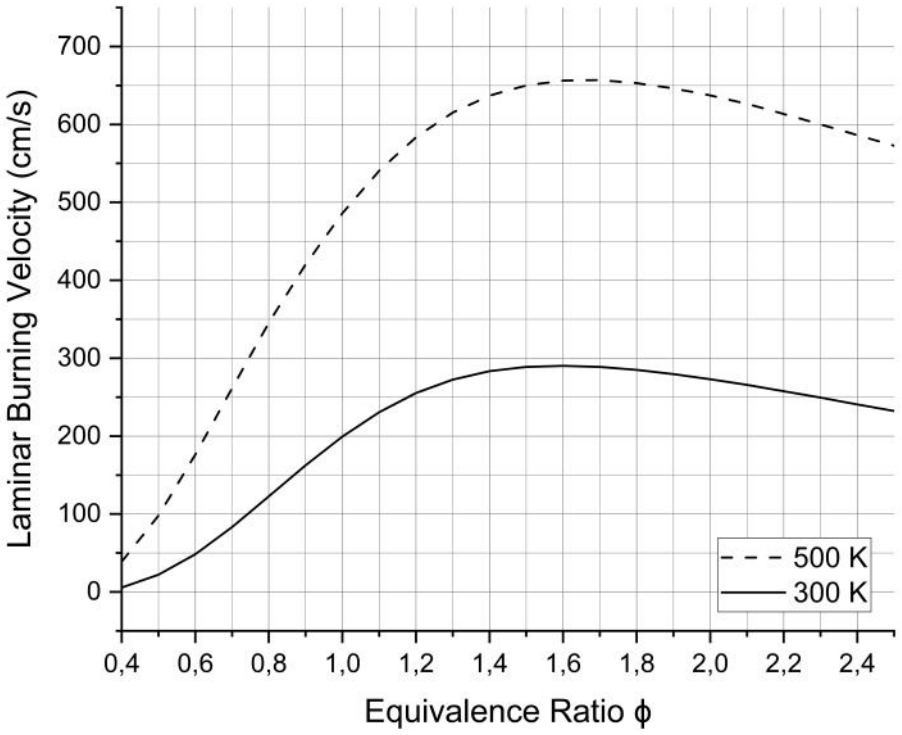

Figure 12: Equivalence Ratio vs. Laminar Burning Velocity: T = 300 & 500 K, P = 5 atm, ϕ = 0.4 - 2.5, Dilution = 0 %

In Figure 12 it is to observe, that higher temperatures increase the laminar burning velocity. In addition to that, the maximum is shifting slightly towards an equivalence ratio of 1.7. This is in line of the expectations, since higher temperatures of the unburned gas is increasing the flame temperature, the chemical reaction rate, the thermal and mass diffusivity and decreases the density. Higher temperatures also improves the flame stability [36]. The temperature 1000 K has been studies, however the speed is much higher compared to the other scenarios, which is why it has been neglected in this graph to ensure a better result presentation.

3.4.5 Effect of the Dilution

The last analysis is the effect of feeding additional N_2 to the system. Only NO_x in the form of NO for two different equivalence ratios have been considered. Also the effect on the laminar burning velocity has been studied. The dilution has been varied from 0 - 20 %.

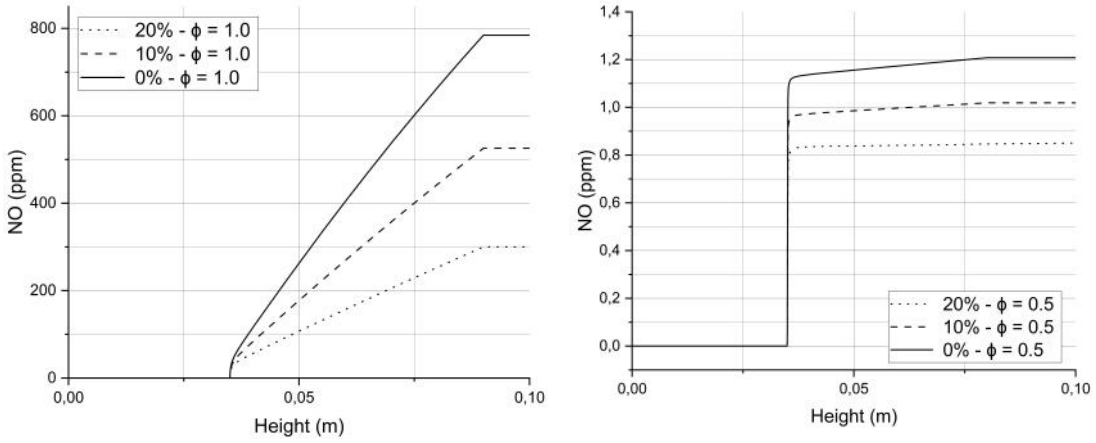

(a) (b)

Figure 13: Dilution Effect: NO (ppm) vs. Burner Height a) Conditions: T = 300 K, P = 5 atm, ϕ = 1.0, Dilution = as stated; b) Conditions: T = 300 K, P = 2 atm, ϕ = 0.5, Dilution = as stated

The dilution effect is clearly notable for $\phi = 1.0$ with lower NO emissions for higher dilution levels (Figure 13 a)). In comparison for leaner combustion increasing the dilution level has only a very small influence on the NO emissions due to already reduced NO emissions caused by the lower combustion temperature (Figure 13 b)). This shows that leaner combustion can achieve lower NO emissions than it can be achieved by increasing dilution levels till up to 20 %. In conclusion, it would be more desirable to run engines under lean combustion conditions instead of increasing the dilution levels.

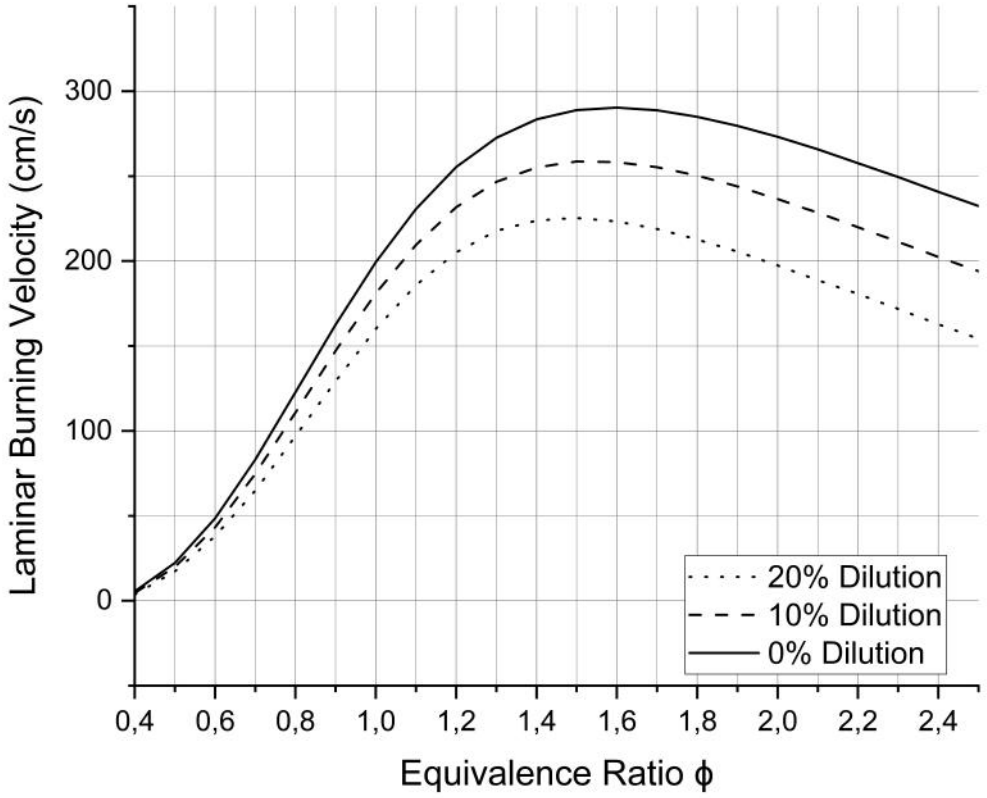

Figure 14: Equivalence Ratio vs. Laminar Burning Velocity: T = 300 K, P = 5 atm, ϕ = 0.4 - 2.5, Dilution = as stated

The laminar burning velocity is gradually decreasing for increasing dilution levels from 2.029 to 1.60 m/s for a dilution of 20 %, also shown in Figure 14. The additional N_2 is reducing the amount of flammable gases and therefore, lowering the combustion temperature and chemical reactivity of the mixture, which is again reducing the laminar burning velocity.

3.5 Sensitivity of Hydrogen Combustion Reactions

The following Figure 15 is showing the important reactions of hydrogen combustion at the highest temperature inside the chamber under the defined reference conditions.

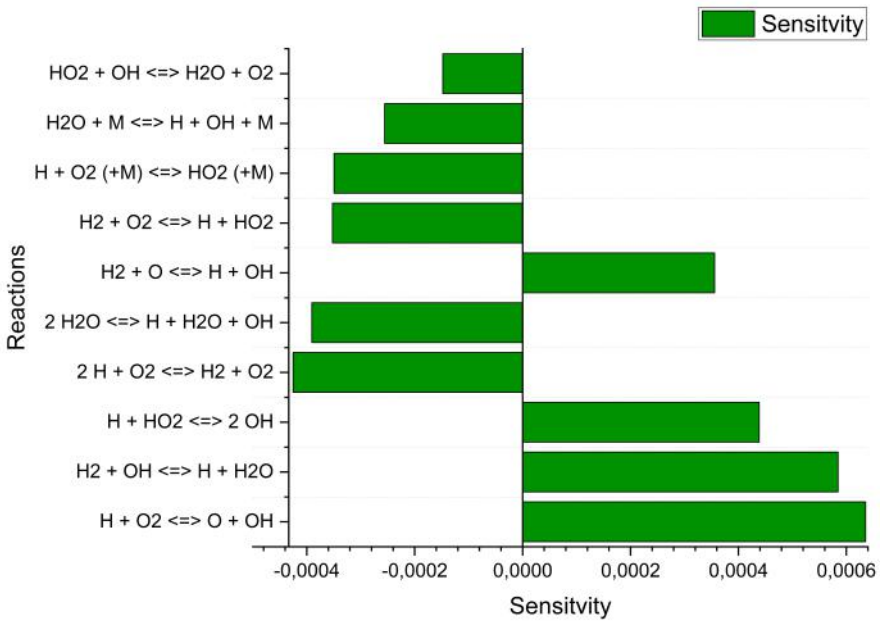

Figure 15: Chemical Reactions vs. Sensitivity: T = 300 K, P = 5 atm, ϕ = 1.0, Dilution = 0 %

The reactions with the highest sensitivity is a chain branching reaction (H + O_2 <=> O + OH), one radical and one molecule form two radicals. The second highest positive sensitivity is a chain propagating reaction (H_2 + OH <=> H + H_2O), the amount of radicals in the flame stay constant, one radical is consumed, while another one is produced by releasing energy. When the radicals inside the flame increase the reactivity / the reaction rate of the combustion increases. In contrary, the reaction with the highest negative sensitivity (2H + O_2 <=> H_2 + O_2) is a chain terminating reaction, which means radicals are converted into molecules and therefore, the reactivity decreases [37].

4 Experiments

In this section all segments of the physical experiments in the laboratory are described, beginning with the experimental setup, over to the validation matrix, to schlieren imaging and to the post-processing of the experimental data.

4.1 Experimental Setup

Figure 16 below shows the experimental set up of the constant volume chamber with all its components and describes the working procedure and work flow. A photograph of the real laboratory experimental setup can be found in Appendix A8.

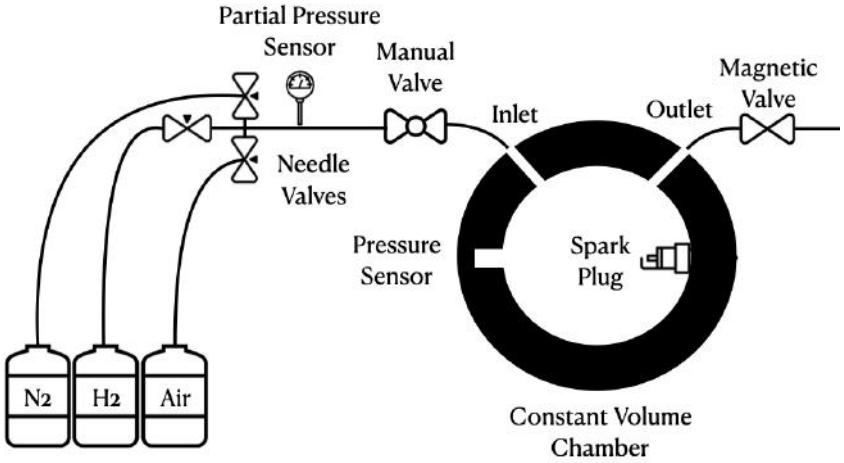

Figure 16: Experimental Setup

The constant volume chamber is build by the laboratory team of the Energy Conversion Team under Professor Martti Larmi. One steel plate with glass windows on each side form the outer walls of the combustion chamber. The windows have a diameter of 120 mm, while the chamber size is of 190 mm and the steel plate thickness is around 68 mm. The chamber itself has the same diameter as the windows and a thickness of about 30 mm.

The chamber consists of an inlet, to feed the gas mixture and an outlet, from where the burned mixture is flushed out. A pressure sensor is installed on the opposite side of the spark plug inside the chamber to measure the pressure rise during the combustion. The spark plug likewise contains a pressure sensor, with the two sensors on the opposite sides of the chamber it is possible to see pressure delays inside the chamber. The chamber is connected on the outlet side with a magnetic valve, which will be opened manually after the combustion took place. The inlet side is connected with three needle valves to feed the gas mixture and a manual ball valve, which will be closed, when the desired partial pressure ratio is reached inside the constant volume chamber. The ball valve, the needle valves and the connecting components are from Swagelok. The magnetic valve from ASVO and the partial pressure sensor

utilized to measure the pressure of the mixture fed into the chamber is from Trafag. The partial pressure sensor has a range from 0 to 10 bar with an accuracy of 0.01 bar. The human accuracy for adjusting the partial pressures manually is found to be 0.01 bar. The installed spark plug is from AVL - Bosch.

The gas mixture is reached by two / three different gas bottles. For the dilution scenario firstly N_2, secondly H_2 and lastly air is supplied into the chamber according to the desired air / fuel ratio. In case of the zero dilution measurements only H_2 and premixed synthetic air are fed into the chamber. After the combustion, the gases are released and the chamber flushed first with N_2 and then with air from the gas bottle to ensure atmospheric air pressure inside the chamber. The purity of the gases are 99.2 % for N_2, 99.1 % for H_2 and 99.2 % for air.

The imagining technique used for this experimental setup is called Z-Schlieren method, for which the mode of operation is described in Subsection 4.3. The components used in the Z-Schlieren setup are a white LED point light source from SugarCUBE Ultra, a razor blade to visualize the density differences and the FASTCAM SA-Z camera from Photron. The camera has a frame rate of 3000 frames / second, a shutter speed of 1/200000 seconds, a Zoom ratio of 47.6 % and a Resolution of 1024x1024. Within the combustion process a total number of 200 frames are taken. The pressure sensors are communicating with DEWESoft, where the recordings can be managed. The recording starts in slow record mode with 100 Hz for the charging period and increases to 20000 Hz after the trigger has been set off. The spark and the exhaust valve are operated with a LabView Panel.

4.2 Validation Matrix

The validation matrix (Table 3) is defined similarly to the simulation matrix in Section 3. It states the test conditions of the experimental research to compare and validate the results found by Cantera. The reference scenario is defined as previously: T = 300 K, P = 5 bar, $\phi = 1.0$, Dilution of 0 %.

Variables	**Value 1**	**Value 2**	**Value 3**
Fuel Composition:	Air + H2		
Temperature:	300 K		
Pressure:	5 & 10 bar		
Equivalence Ratio:	0.4 - 1.4 in 0.2 steps		
Dilution:	0 %	10 %	20 %

Table 3: Experimental Parameters

The experiments are conducted of three matrices with 27 test points each. The setup is described in Section 4.1. The results are plotted, analysed and discussed in Section 5. Conclusions are drawn and error factors are mentioned in Section 6.

4.3 Schlieren Imaging

Optical diagnostics is used to measure different combustion properties. The effects utilized by optical diagnostics are the light propagation throughout a media. If light hits a homogeneous media, the light propagates uniformly through it. On the other hand disturbances and inhomogeneities redirect the light. This redirection of light can be recognised by optical diagnostic methods like schlieren or OH-radical chemiluminescence. In this thesis the schlieren method is used to imaging the combustion.

A Schliere is defined as a *"relatively-refractive differences within the overall background, and [...] they bend light rays in any direction other than the <normal> direction z"* [38]. With the schlieren method a variation of the medias refractive index can be measured, which means optical inhomogeneities of a transparent media can be measured. The knife egde / razor blade is used to visualize the temperature and density changes (inhomogeneities) in the testing region.

For the experiments of this thesis, a point light (LED laser) source with Z-Schlieren construction, as shown in Figure 17, is used. The name of the structure is given due to the set up of two symmetrical, oppositely tilted parabolic mirrors and the directions of the beam from the source towards the receiver. The testing region, the distance between the mirrors requires a minimum of 2f (f = focal length of the mirror). The light source (lamp) is directed towards the first parabolic mirror, passing through a slit, producing a parallel and collaminated beam through the testing region and towards the second parabolic mirror, where the beam is focused on the camera and the filter (razor blade) [38].

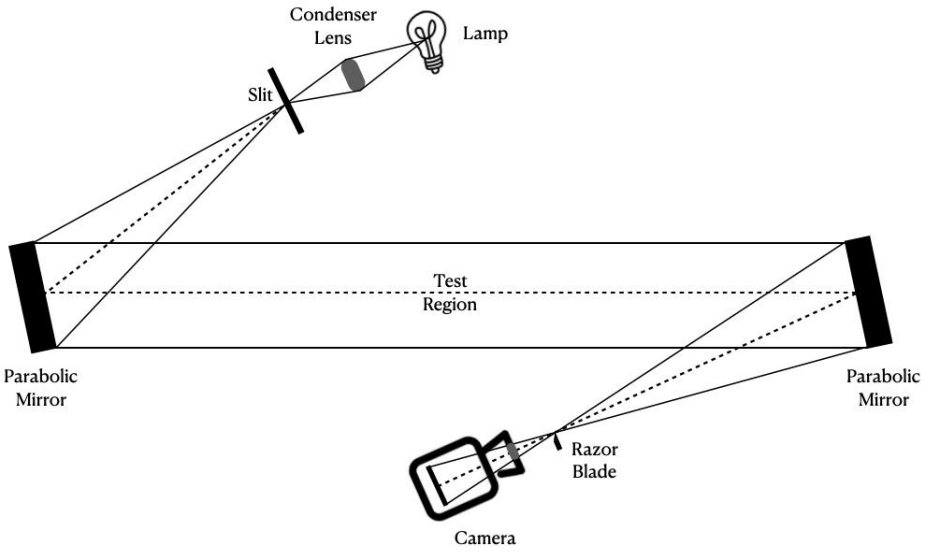

Figure 17: Z-Schlieren Setup [38]

4.4 Post-Processing

The image post-processing has been carried out with MATLAB. Several scripts have been used to process the images taken with the Z-Schlieren technique. One script is reading the images and converting them into an animation in mp4 - format to visualize the taken frames.

Another one takes the images and calculates the flame speed by converting all pixels into black color, removing the background from the images, while calculating the distance between the flame front and the spark plug for each image. By including the time steps between the frames, the specific speed of the flame over each time step, can be calculated. One image of the flame speed calculations can be seen in Figure 18. The processed images are then further edited to gain several plots of the flame front propagation or the flame speed, which are shown and discussed in Section 5.

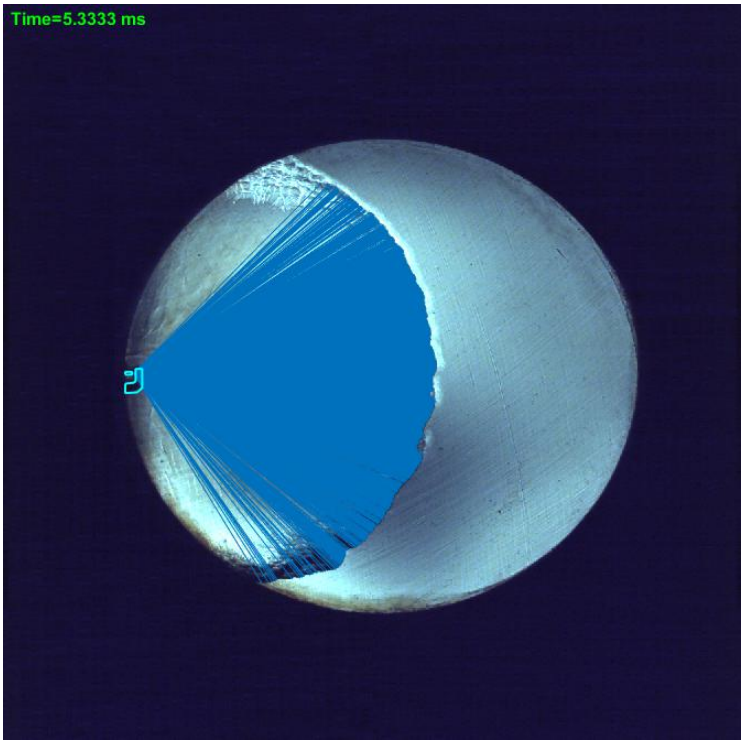

Figure 18: Flame Speed Calculations

Also the data of the pressure rise recorded by DEWESoft is further processed and analysed to be able to understand, when the pressure is increasing and till what peak pressure it is rising. Figure 21 and Figure 22 are summarizing the findings.

5 Results & Analysis

The result and analysis section is distributed into five subsections, which present and discuss the post-processed experimental data gained from the experiments. The subsections are presenting the effect of the equivalence ratio and the dilution, the rise in chamber pressure, the flame front propagation and the flame speed throughout time. Beginning with Section 5.3, a comparison between the reference scenario and the conditions T = 300 K, P = 5 bar, ϕ = 1.0 and dilution = 20 %, are made.

5.1 Experimental Results of the Equivalence Ratio

The following Figure 19 states a comparison of the flame front propagation between different combustion conditions from lean (0.4) to rich (1.4) over time. The chamber conditions are P = 5 bar, T = 300 K, ϕ = as stated and 0 % dilution.

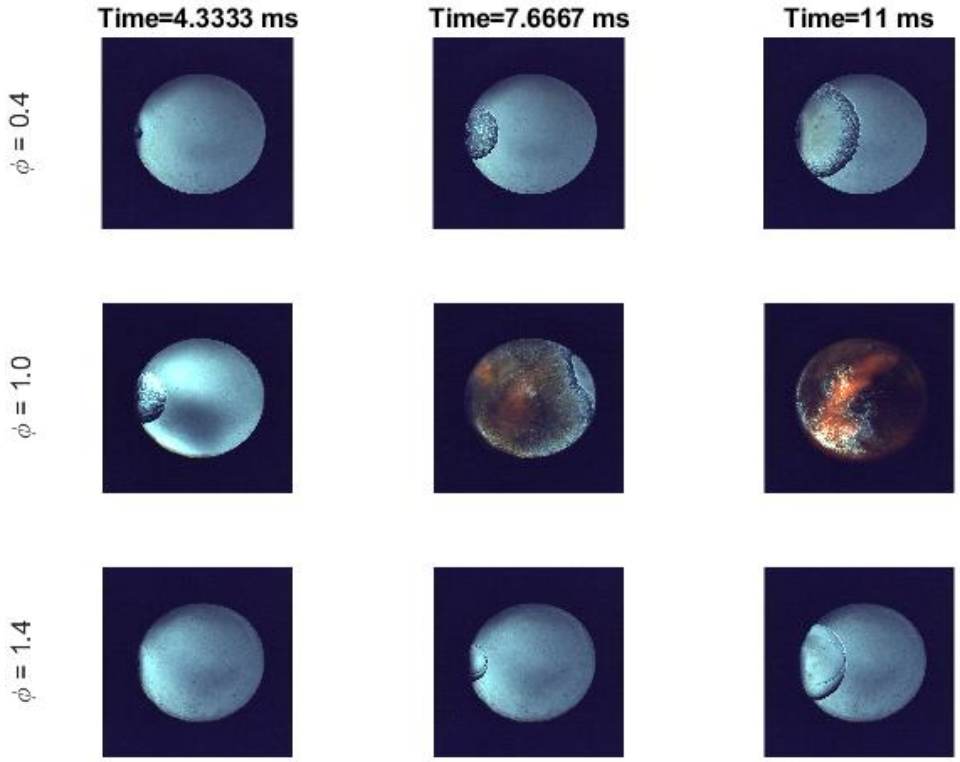

Figure 19: Comparison of the Flame Propagation at different Times after the Ignition - Conditions: T = 300 K, P = 5 bar, ϕ = 0.4 - 1.0 - 1.4, Dilution = 0 %

Figure 19 shows that for lean condition the flame front is propagating with a cellular structure. Whereas, rich conditions burn with a clean flame front. It is to observe, that under stoichiometric conditions, the flame front has already passed, while lean and rich conditions are still in the starting of the combustion process. Here, stoichiometric conditions indicate clearly the presence of turbulences, like wall or window effects. Moreover, yellow jets are shooting from the inlet and outlet of the chamber. Hydrogen combustion is not supposed to display any visible light / yellow

flame. The reason why in this thesis it is visible could have several sources. Firstly the burning of NO_x, secondly of H_2O, or thirdly of metal oxides, originated from rust. We could also observe that rich conditions do not seem to show a faster flame velocity as expected from the Cantera simulations. Within this setup, the combustion was impossible to ignite above an equivalence ratio of 1.4. This might also be related to the experimental setup and combustion conditions.

5.2 Experimental Results of the Dilution

Figure 20 states a comparison of the flame front propagation between different combustion conditions from 0 % to 20 % dilution over time. The chamber conditions are under stoichiometric conditions with P = 5 bar and T = 300 K.

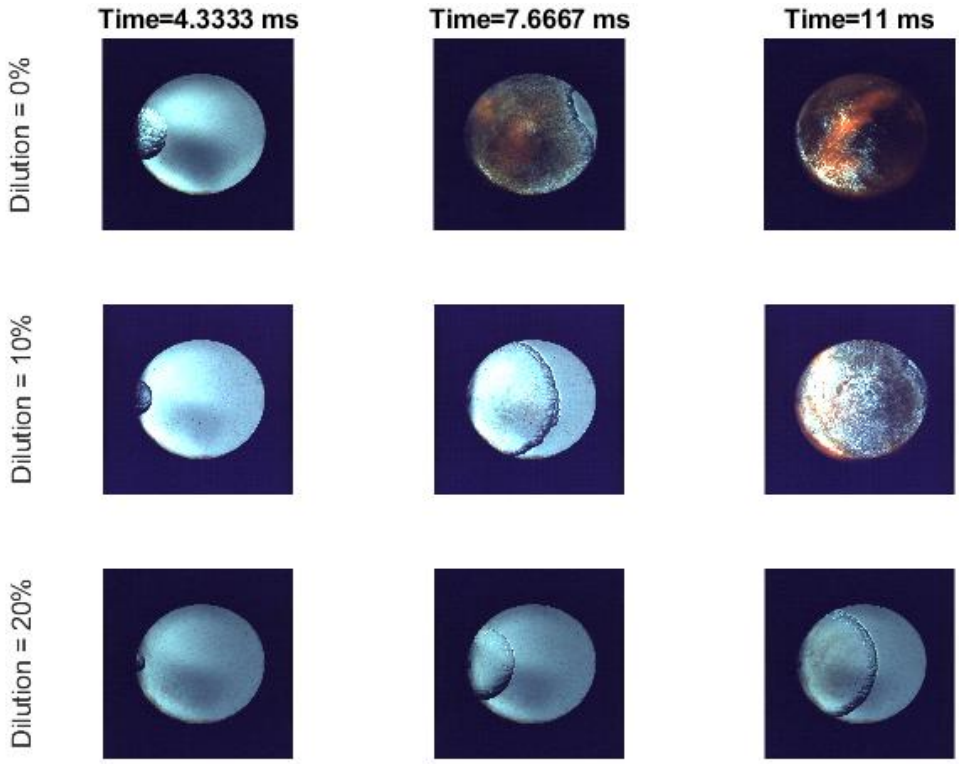

Figure 20: Comparison of the Flame Propagation at different Times after the Ignition - Conditions: T = 300 K, P = 5 bar, ϕ = 1.0, Dilution = 0 - 10 - 20 %

The Figure shows, that an increase in dilution (N_2) is decreasing the flame velocity. This result is in line with the Cantera simulations of the dilution effect from Section 3.4.5, which states that higher N_2 levels decrease the combustion temperature and chemical reactivity of the mixture, concluding in a reduced burning velocity.

5.3 Experimental Results of the Chamber Pressure

For all the test points an increase in chamber pressure and chamber temperature can be observed, which is caused by the heat release from the strongly exothermic combustion reactions [39]. The following figures show the pressure increase over time for the given conditions. A similar graph can be obtained for every other test point of the validation matrix.

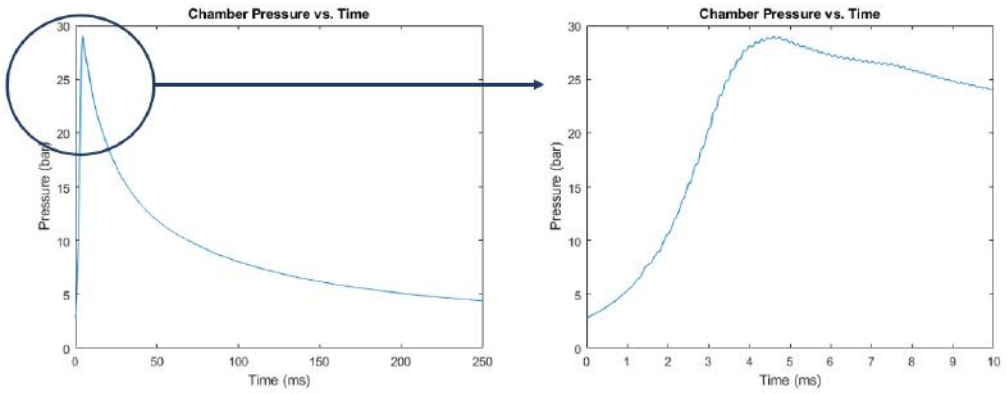

Figure 21: Chamber Pressure vs. Time - Reference Conditions (T = 300 K, P = 5 bar, ϕ = 1.0, Dilution = 0 %)

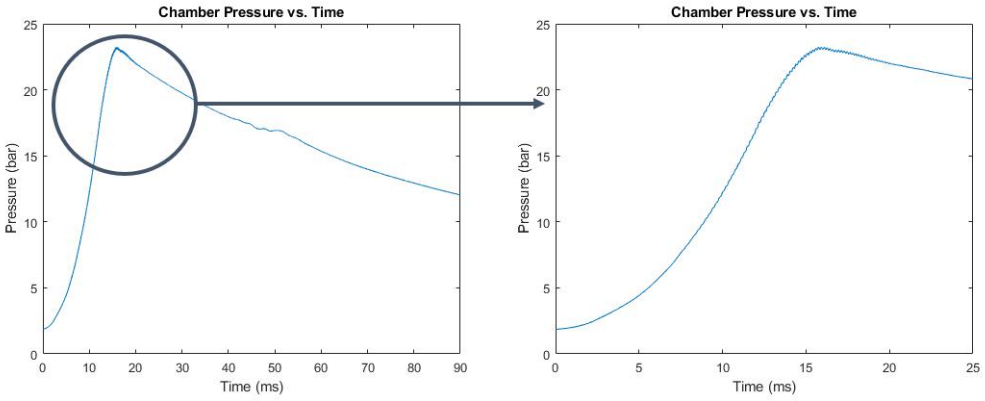

Figure 22: Chamber Pressure vs. Time - Conditions: T = 300 K, P = 5 bar, ϕ = 1.0, Dilution = 20 %

For each figure, the left side represents the chamber pressure over a longer time period (Figure 21 = 250 ms; Figure 22 = 90 ms), while the right side of zooms in and displays only a short time period (Figure 21 = 10 ms; Figure 22 = 25 ms). Under reference conditions a maximum pressure of 29 bar is reached at 4.6 ms after the ignition of the gas mixture, whereas the scenario with 20 % dilution peaks at 15.75 ms with a pressure of 23.3 bar. The fast drop in chamber pressure is traced back to the large amount of heat transfer of the experimental setup presented for this thesis. This is caused by the lack of preheating of the chamber and large window area.

5.4 Experimental Results of the Flame Front

In a next step the progressing of the flame front has been studied. The graph shows how the flame front is propagating from one side of the chamber to the other, throughout the combustion process.

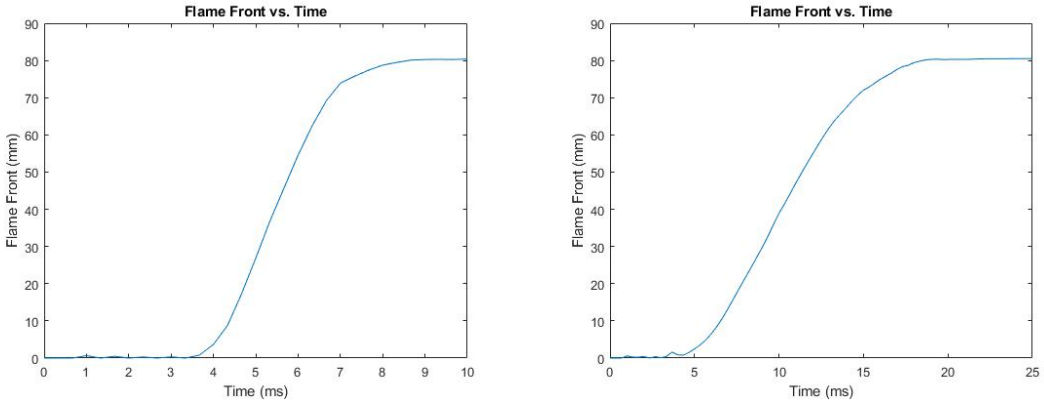

(a) (b)

Figure 23: Flame Front vs. Time a) Reference Conditions: T = 300 K, P = 5 bar, ϕ = 1.0, Dilution = 0 %; b) Conditions: T = 300 K, P = 5 bar, ϕ = 1.0, Dilution = 20 %

For the calculations it was assumed that the maximum value between the spark plug / previous location of the flame front and the new location of the flame front is used as a conform entire flame front. This has been executed for each frame to calculate the maximum absolute distance. After a certain amount of frames, when the flame front propagation is not homogeneous anymore, some error factor is introduced to the graph. The maximum distance is reached, when hitting the other end of the chamber. When comparing the left with the right figure, as expected the flame front of the combustion under reference conditions is faster compared to the flame front of the combustion with dilution.

5.5 Experimental Results of the Flame Speed

The Figure 24 shows the variation of burning velocity over the time, displayed by observed velocity from one frame to another.

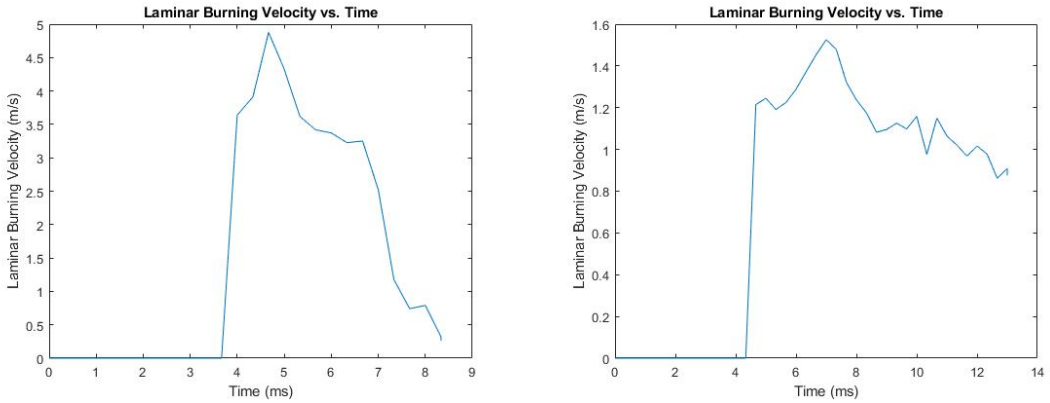

(a) (b)

Figure 24: Burning Velocity per frame vs. Time a) Reference Conditions: T = 300 K, P = 5 bar, $\phi = 1.0$, Dilution = 0 %; b) Conditions: T = 300 K, P = 5 bar, $\phi = 1.0$, Dilution = 20 %

The velocity is calculated from the post-processing program as described in the Section 4.4. The graph merges the different burning velocities per frame. For reference conditions it shows the start of the combustion process around 3.7 ms and the peak at 4.6 ms with a peak velocity of 4.87 m/s. Under 20 % dilution conditions the start of the combustion shifts the start and the peak towards 4.2 ms (start) and 7 ms (peak) with a velocity of 1.5 m/s. In the following paragraph the flame speed has been further processed. This has only be carried out for reference conditions. Hereby, the part which can be assumed to be realistic values for the burning velocity is used for averaging calculations to gain a single value for the flame speed.

Figure 25 shows a comparison of the data gathered from the experiments with the simulations in Cantera. The graph shows the trend of the flame speed over the equivalence ratio. The graph showing only the experimental data can be found in the Appendix A9.

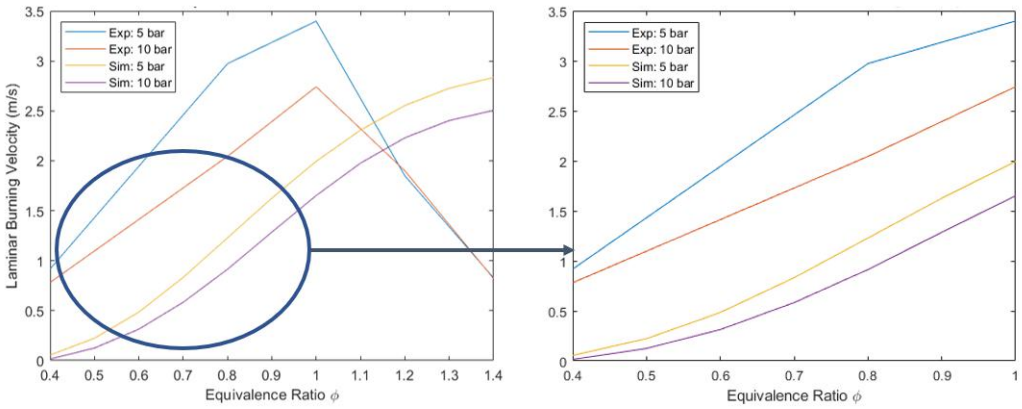

Figure 25: Comparison of Equivalence Ratio vs. Flame Speed - Conditions: T = 300 K, P = as stated, ϕ = 1.0, Dilution = 0 %

The flame speed was found by averaging the flame speed over a certain threshold, specifically defined for each scenario. The averaging increases the uncertainty and error factor in the system. It is to observe, that the simulations and experiments are not matching. While the experiments peak around and equivalence ratio of 1.0 - 1.1, is the peak for the simulations expected around 1.6. When we have a closer look at the lean combustion side, the graphs show a similar trend for 5 and 10 bar. In the 5 bar case there is a runaway point at an equivalence ratio of 0.8. Apart from that the figure states, that the flame speed decreases for higher pressures and that the flame speed increases for higher equivalence ratios, under the requirement that the equivalence ratio is before the peak. Simulation and experimental results show an offset, which could also be observed by Pareja (2010) [23].

6 Conclusions & Further Investigations

Coming back to the research questions from Section 1.2:

- Question 1) How to measure the hydrogen combustion flame front propagation with schlieren method in a constant volume combustion bomb?

  This is answered in detail in Section 4.3 and represented best by Figure 17 (reproduced below), where the schematics of the Z-Schlieren setup is shown and explained.

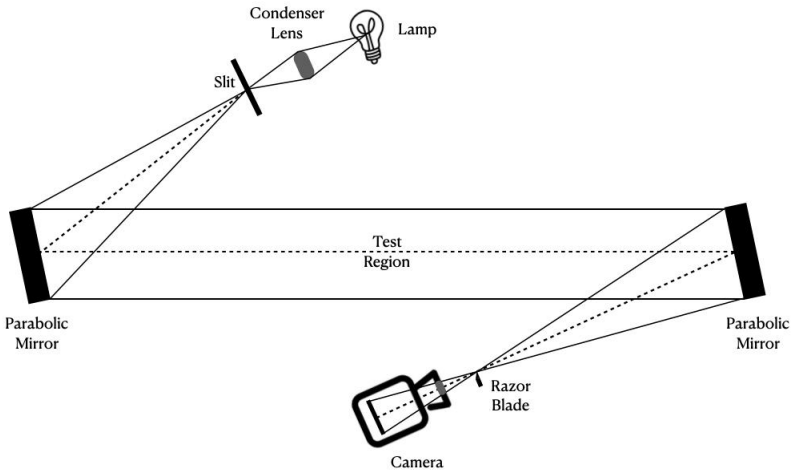

  Generally, variations of the medias optical homogeneities can be measured. The razor blade visualizes the temperature and density changes (inhomogeneities) in the testing region. For this thesis a white point light (LED laser) source has been utilized.

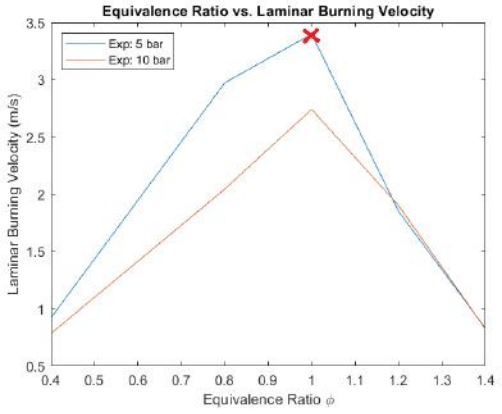

  The measured flame speed for the reference scenario was found to be 3.4 m/s.

- Question 2) How do various parameters, like initial temperature, pressure, dilution, and relative air-to-fuel ratio (λ) or equivalence ratio (ϕ) affect the flame speed?

  The effects of initial chamber pressure, initial mixture temperature, equivalence ratio and N_2 dilution are discussed in detailed in Section 5, an overview is displayed in Table 4. The study shows that, with increasing initial chamber pressure the flame speed is decreasing, with increasing mixture temperature the flame speed is increasing, the increasing dilution factor is decreasing the flame speed and the equivalence ratio depends, if the equivalence ratio is before the peak velocity or beyond.

  Influencing Factors and Effects:

Parameter	**Change of Parameter**	**Effect on Flame Speed**
Pressure:	↑	↓
Temperature:	↑	↑
Equivalence Ratio*:	0.4 - 1.6	↑
Equivalence Ratio*:	1.6 - 2.5	↓
Dilution:	↑	↓

Table 4: Overview of Influencing Factors

*The statement over the equivalence ratio is made by taking into consideration the findings of the Cantera simulations. For a clear statement the effects of the equivalence ratio needs to be further tested and studied.

- Question 3) How do the measurements compare with laminar flame speed computations?

  The analysis can be found in Section 5.5, which states that the simulations and experiments match to some extend before reaching stoichiometric conditions. There is a runaway point at $\phi = 0.8$ and an offset in y-direction. While, for equivalence ratios higher than 1, the measurements are not matching the computations. That the simulations and the experiments are not matching precisely can have several reasons, from human errors to component unsuitability or mixture related issues.

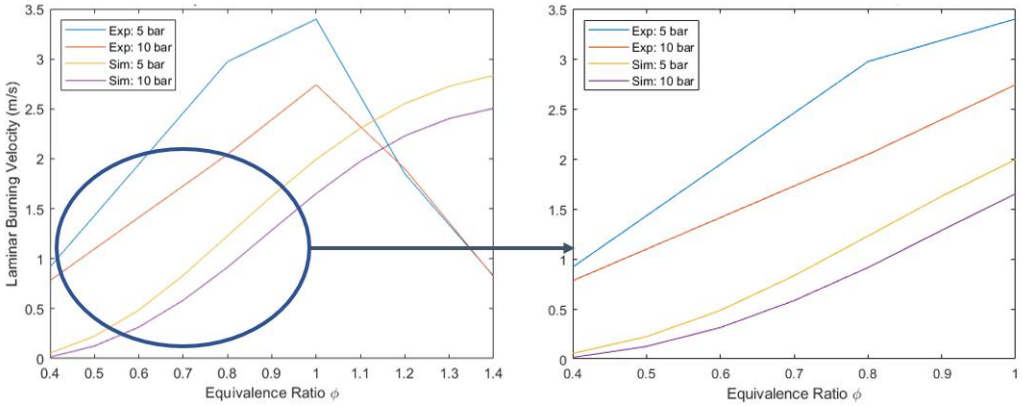

Error Factors and Improvements:

The biggest human error factor is the generation of the mixture through the manual inlet valves. Within these samples the maximum accuracy is about 0.01, which can be improved through an automatic feeding system for future studies. In addition, the frequency of cleaning the chamber might have an impact on the measurements, since some residues of the cleaning liquid could be combusted or residual gases and grease inside the pipes and valves, which have not been cleaned or flushed out correctly, could falsify the measurements.

After man-made mistakes also mixture specific errors could occur, for example the mixture homogeneity. With this setup it is not possible to know the mixture content inside the chamber. Only from the schlieren imagining it can be assumed if the mixture is mixed properly or if different gas layers exist. In the future additional tests with different waiting times between charging and combusting of the mixture or a computational fluid dynamic model of the mixing process can be used to understand the impact of the mixture homogeneity. Against the expected, the combustion of hydrogen emitted visible light. This could have several reasons as mentioned in section 5.1. To determine the reason, wavelength filters can be used, which will help to understand the nature of the yellow flame.

The frame rate could be increased to improve the measuring conditions. More detailed recording would be possible. Currently, the chamber is not heated. Heating up the chamber is decreasing the temperature difference between the chamber and the combustion temperature and therefore, the heat transfer. It could also enhance the combustion, which would expand the validation matrix. The conditions of the measurements are rather low pressure measurements, widening the pressure range could be beneficial in future research.

Equipment related issues are for example the size of the chamber. The chamber is very small comparably to the big windows, which leads to a high amount of heat transfer. This is possibly the explanation for the fast pressure drop in the chamber after the combustion. To decrease the heat transfer to the surroundings,

additional insulation can be attached. Increasing the chamber size and decreasing the window size is also advantageous. Another problem in relation to the small chamber, are the windows and the wall effects, which can affect the flame front, when hitting them. Moreover, the purity of the gases is not of the highest quality. The remaining percent, which is not pure hydrogen, air or nitrogen, is unknown. These gases could increase or decrease the burning velocity. For the future it is recommended to use higher quality gases to exclude this uncertainty. After operating the combustion chamber for a very short time, the steel in the inside of the chamber started oxidizing. The effect of the oxidizing and if the rust is taking part in the combustion is unknown. It could also be proven that the design of the chamber is not optimal, since jets from the inlet and outlet can be observed. Henceforth, valves could be placed closer to the chamber to reduce the space, where gases accumulate in the pipes. During the measurements some pressure sensor axis changes could be noticed. Eventually the scale also changed slightly, which could have caused an imprecise charging of the gas mixture.

In the MATLAB code the distance and therefore, the velocity is averaged. Plus not all pixels can be identified since impurities, background or combustion noise makes it hard to differentiate the flame front from the background. Also after a certain number of frames, jets and other turbulences are impacting the velocity. In the future the MATLAB program could be refined and threshold values customized. Currently, the strain and the curvature of the flame (stretch) is not considered inside the calculations, which needs to be implemented for future studies. In addition, Cantera might not be the right choice for these kind of comparisons between simulations and experiments, since Cantera is simplifying many aspects of the flame speed calculations and assuming the gas mixture to be ideal, without the possibility to input any stretch.

Generally, it could be favorable to increase the number of repetitions to decrease the error variation. It is to say, that the experiments are not purely laminar as seen by the schlieren imaging. For clarity, the Reynolds number can be calculated and compared to the number for laminar burning velocity. All the factors above explain, why the experimental data is not matching the Cantera simulations or literature.

7 References

[1] NRDC. "Fossil Fuels: Dirty Facts." (), [Online]. Available: https://www.nrdc.org/stories/fossil-fuels-dirty-facts. accessed: 30.03.2022.

[2] I. E. Agency, "Co2 emissions worldwide," 2019. [Online]. Available: https://www.iea.org/data-and-statistics/data-browser?country=WORLD&fuel=CO2%20emissions&indicator=CO2BySector.

[3] S. Verhelst and T. Wallner, "Hydrogen-fueled internal combustion engines," *Progress in energy and combustion science*, vol. 35, no. 6, pp. 490–527, 2009.

[4] IEA. (), [Online]. Available: https://www.iea-amf.org/content/fuel_information/ammonia. accessed: 02.05.2022.

[5] H. Lesmana, Z. Zhang, X. Li, M. Zhu, W. Xu, and D. Zhang, "Nh3 as a transport fuel in internal combustion engines: A technical review," *Journal of Energy Resources Technology*, vol. 141, no. 7, 2019.

[6] J. Warnatz, U. Maas, R. W. Dibble, and J. Warnatz, *Combustion*. Springer, 2006.

[7] R. Stephen, "Turns. an introduction to combustion: Concepts and applications," *Mechanical Engineering Series. McGraw Hill,*, 2000.

[8] T. Poinsot and D. Veynante, *Theoretical and numerical combustion*. RT Edwards, Inc., 2005.

[9] E. Energy. (), [Online]. Available: https://www1.eere.energy.gov/hydrogenandfuelcells/tech_validation/pdfs/fcm03r0.pdf. accessed: 15.03.2022.

[10] H. L. Yip, A. Srna, A. C. Y. Yuen, *et al.*, "A review of hydrogen direct injection for internal combustion engines: Towards carbon-free combustion," *applied sciences*, vol. 9, no. 22, p. 4842, 2019.

[11] L. M. Gandia, G. Arzamendi, and P. M. Diéguez, *Renewable hydrogen technologies: production, purification, storage, applications and safety*. Newnes, 2013.

[12] P. F. C. Dataset. (), [Online]. Available: https://paperswithcode.com/dataset/pem-fuel-cell-dataset. accessed: 30.03.2022.

[13] Y. Manoharan, S. E. Hosseini, B. Butler, *et al.*, "Hydrogen fuel cell vehicles; current status and future prospect," *Applied Sciences*, vol. 9, no. 11, p. 2296, 2019.

[14] E. Abohamzeh, F. Salehi, M. Sheikholeslami, R. Abbassi, and F. Khan, "Review of hydrogen safety during storage, transmission, and applications processes," *Journal of Loss Prevention in the Process Industries*, vol. 72, p. 104 569, 2021.

[15] G. Pearson, M. Leary, A. Subic, and J. Wellnitz, "Performance comparison of hydrogen fuel cell and hydrogen internal combustion engine racing cars," in *Sustainable automotive technologies 2011*, Springer, 2011, pp. 85–91.

[16] I. Staffell, D. Scamman, A. V. Abad, *et al.*, "The role of hydrogen and fuel cells in the global energy system," *Energy & Environmental Science*, vol. 12, no. 2, pp. 463–491, 2019.

[17] H. Fayaz, R. Saidur, N. Razali, F. Anuar, A. Saleman, and M. Islam, "An overview of hydrogen as a vehicle fuel," *Renewable and Sustainable Energy Reviews*, vol. 16, no. 8, pp. 5511–5528, 2012.

[18] A. Ajanovic, M. Sayer, and R. Haas, "The economics and the environmental benignity of different colors of hydrogen," *International Journal of Hydrogen Energy*, 2022.

[19] H. Bulletin. (), [Online]. Available: `https://www.h2bulletin.com/knowledge/hydrogen-colours-codes/`. accessed: 18.03.2022.

[20] Hyperphysics. (), [Online]. Available: `http://hyperphysics.phy-astr.gsu.edu/hbase/Kinetic/idegas.html`. accessed: 09.03.2022.

[21] Cantera. (), [Online]. Available: `https://cantera.org/science/flames.html`. accessed: 09.03.2022.

[22] R. J. Kee, M. E. Coltrin, and P. Glarborg, *Chemically reacting flow: theory and practice*. John Wiley & Sons, 2005.

[23] J. Pareja, H. J. Burbano, and Y. Ogami, "Measurements of the laminar burning velocity of hydrogen–air premixed flames," *International Journal of Hydrogen Energy*, vol. 35, no. 4, pp. 1812–1818, 2010.

[24] A. Bhattacharya, "Analysis of laminar premixed flame structure of isooctane/2-methylfuran/air mixtures with a skeletal mechanism," *Combustion Theory and Modelling*, vol. 25, no. 7, pp. 1211–1244, 2021. [Online]. Available: `https://doi.org/10.1080/13647830.2021.1970231`.

[25] A. Frassoldati, T. Faravelli, and E. Ranzi, "A wide range modeling study of nox formation and nitrogen chemistry in hydrogen combustion," *International Journal of Hydrogen Energy*, vol. 31, no. 15, pp. 2310–2328, 2006.

[26] C. Olm, I. G. Zsély, R. Pálvölgyi, *et al.*, "Comparison of the performance of several recent hydrogen combustion mechanisms," *Combustion and Flame*, vol. 161, no. 9, pp. 2219–2234, 2014.

[27] U. B. M. Engineering. (), [Online]. Available: `https://me.berkeley.edu/gri_mech/`.

[28] C. M. Group. (), [Online]. Available: `http://creckmodeling.chem.polimi.it/menu-kinetics/menu-kinetics-detailed-mechanisms`. accessed: 18.03.2022.

[29] Q.-D. Wang, Y. Sun, and H. J. Curran, "Comparative chemical kinetic analysis and skeletal mechanism generation for syngas combustion with no x chemistry," *Energy & Fuels*, vol. 34, no. 1, pp. 949–964, 2019.

[30] N. Galway. (), [Online]. Available: `http://c3.nuigalway.ie/combustionchemistrycentre/mechanismdownloads/`. accessed: 18.03.2022.

[31] U. S. Diego. (), [Online]. Available: https://web.eng.ucsd.edu/mae/groups/combustion/mechanism.html. accessed: 18.03.2022.

[32] A. A. Konnov, "Yet another kinetic mechanism for hydrogen combustion," *Combustion and Flame*, vol. 203, pp. 14–22, 2019.

[33] Capriolo, Brackmann, L. Lavadera, Methling, and Konnov, "An experimental and kinetic modeling study on nitric oxide formation in premixed c3 alcohols flame," *Proceedings of the Combustion Institute*, vol. 38, pp. 805–812, 2021. [Online]. Available: https://www.sciencedirect.com/science/article/pii/S1540748920304831.

[34] C. K. Law, *Combustion physics*. Cambridge university press, 2010.

[35] F. Biagioli and F. Güthe, "Effect of pressure and fuel–air unmixedness on nox emissions from industrial gas turbine burners," *Combustion and Flame*, vol. 151, no. 1-2, pp. 274–288, 2007.

[36] J. Natarajan, T. Lieuwen, and J. Seitzman, "Laminar flame speeds of h2/co mixtures: Effect of co2 dilution, preheat temperature, and pressure," *Combustion and flame*, vol. 151, no. 1-2, pp. 104–119, 2007.

[37] C. Forum. (), [Online]. Available: https://chem.libretexts.org/Bookshelves/Physical_and_Theoretical_Chemistry_Textbook_Maps/Supplemental_Modules_(Physical_and_Theoretical_Chemistry)/Kinetics/04%3A_Reaction_Mechanisms/4.03%3A_Chain_Reactions_I. accessed: 18.03.2022.

[38] G. S. Settles, *Schlieren and shadowgraph techniques: visualizing phenomena in transparent media*. Springer Science & Business Media, 2001.

[39] M. Kuznetsov, S. Kobelt, J. Grune, and T. Jordan, "Flammability limits and laminar flame speed of hydrogen–air mixtures at sub-atmospheric pressures," *International journal of hydrogen energy*, vol. 37, no. 22, pp. 17 580–17 588, 2012.

A Appendix

Mechanism Validation:

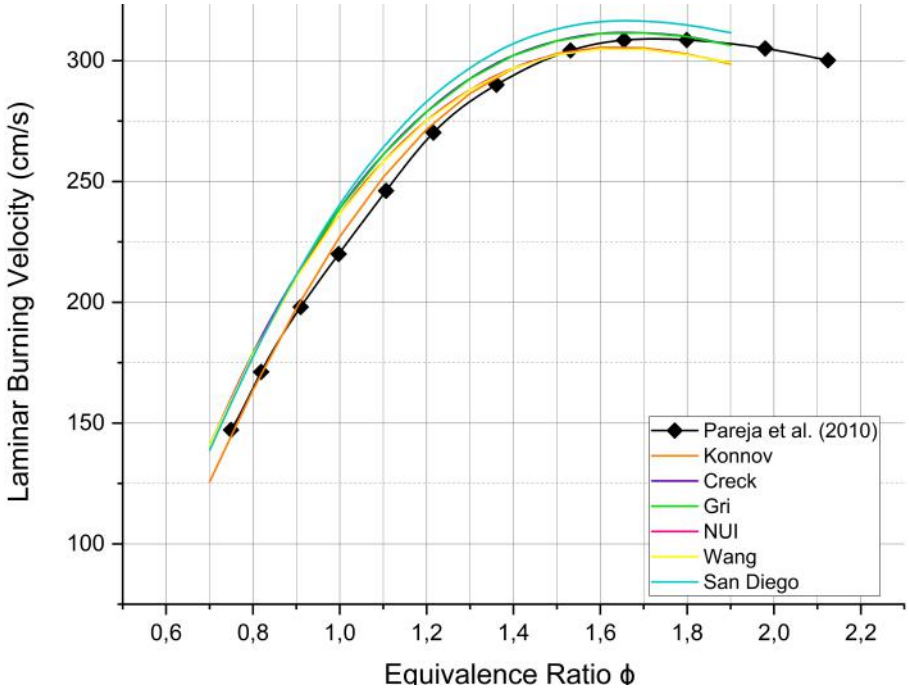

Figure A1: H2 + Air Combustion

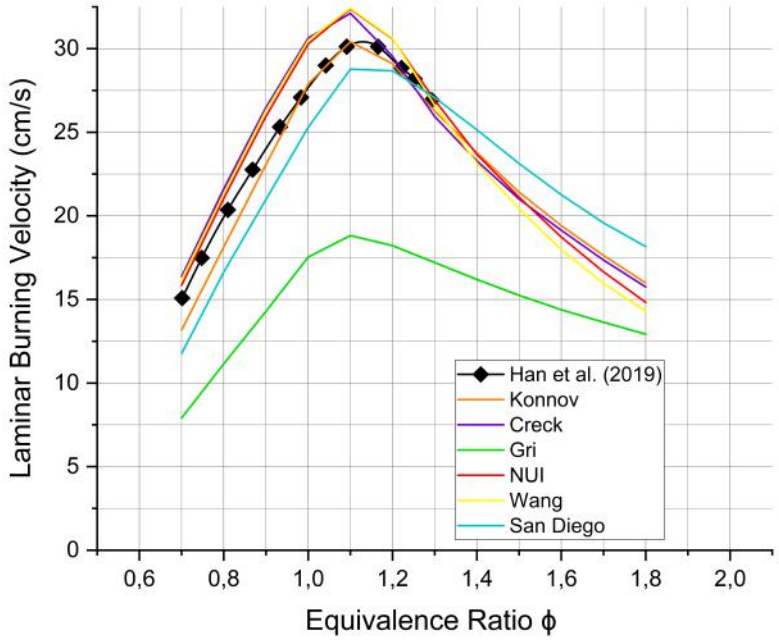

Figure A2: H2 + NH3 + Air Combustion

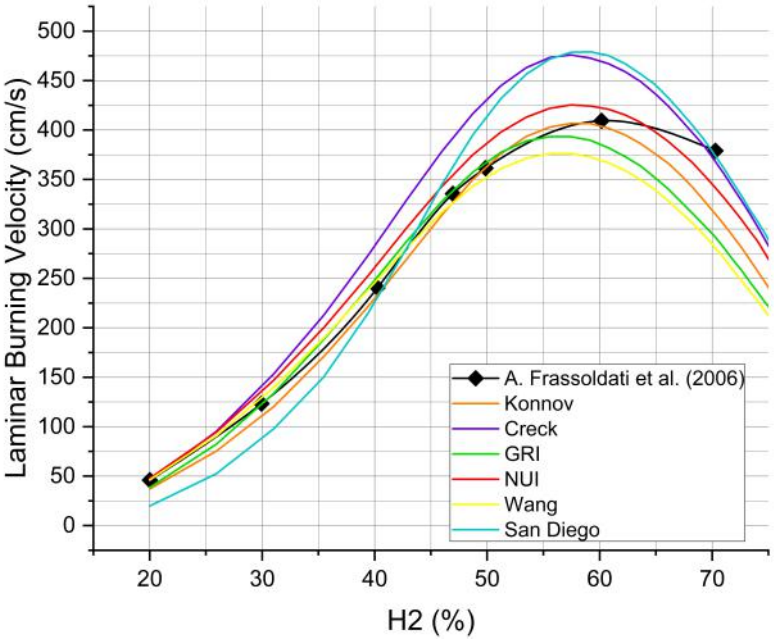

Figure A3: H2 + N2O Combustion

Pressure Effect:

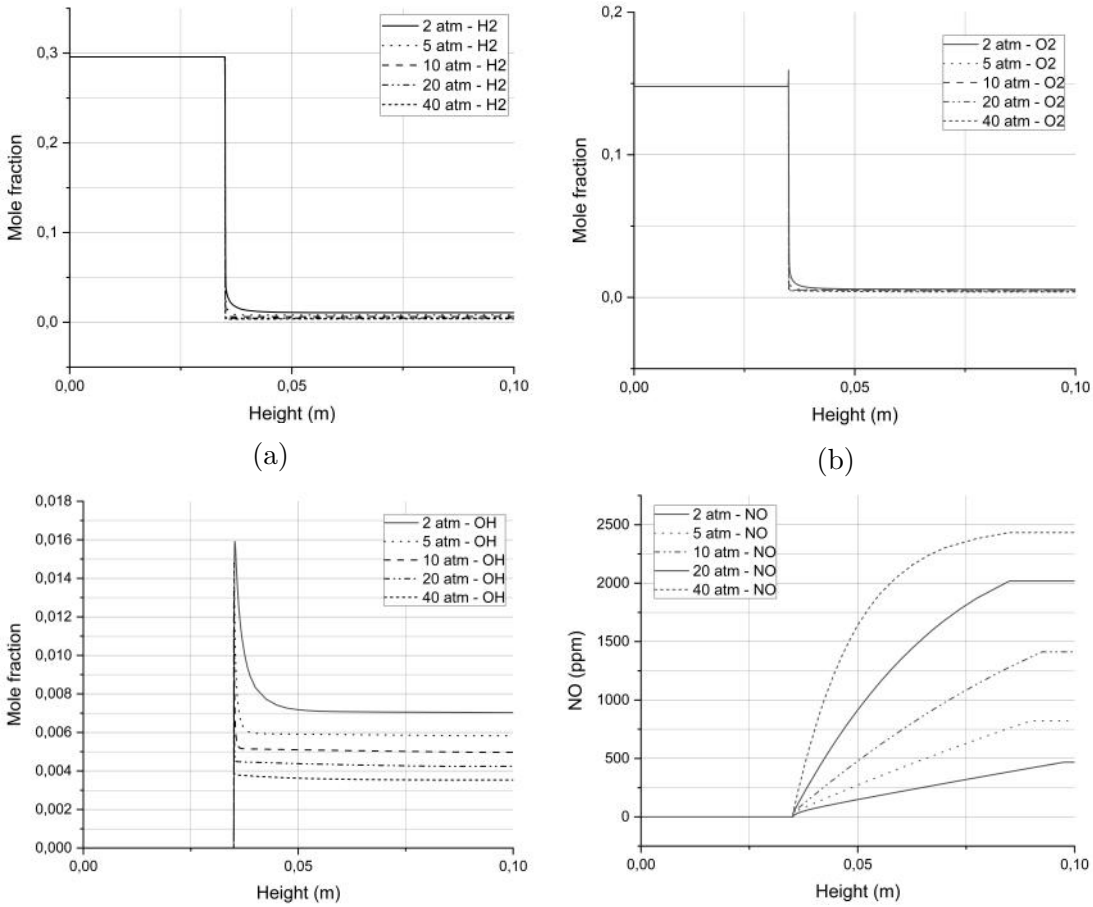

Figure A4: Pressure Effect Extended

Temperature Effect:

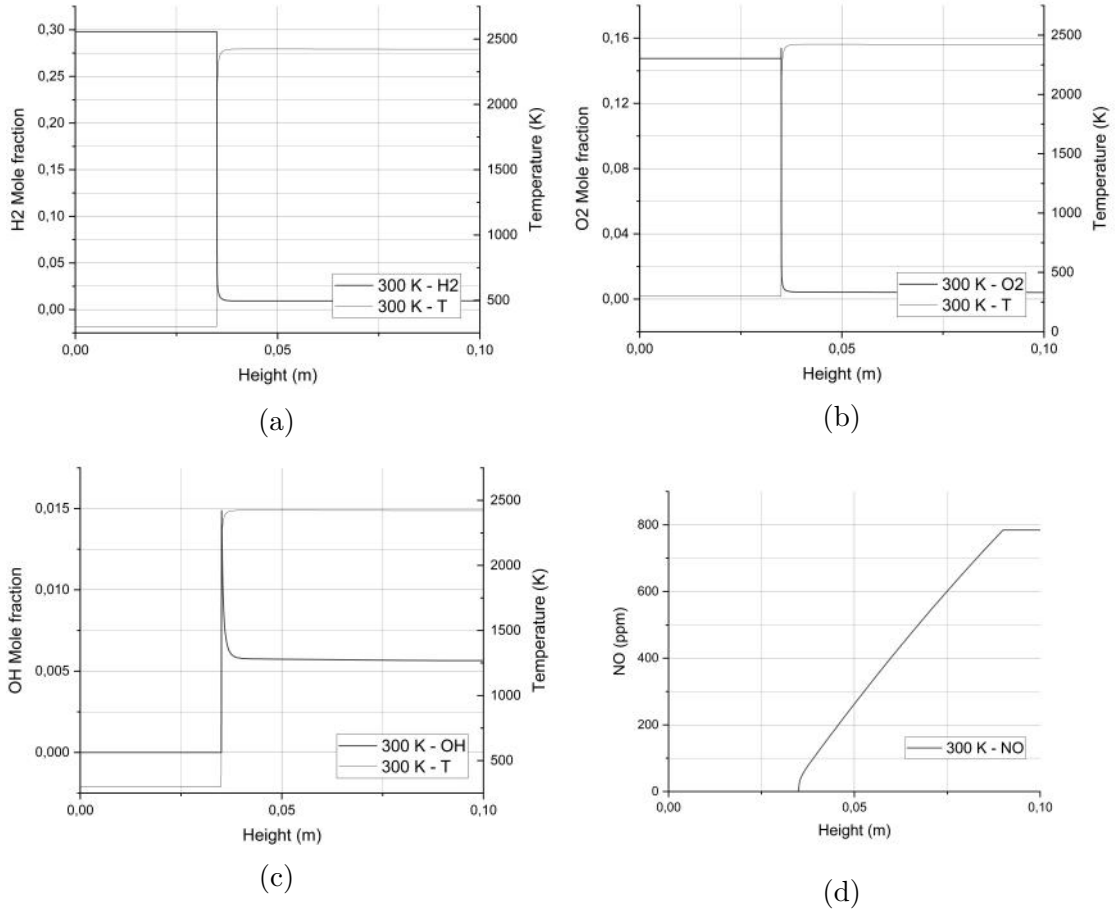

Figure A5: Extensive Analysis 300 K

Temperature Effect:

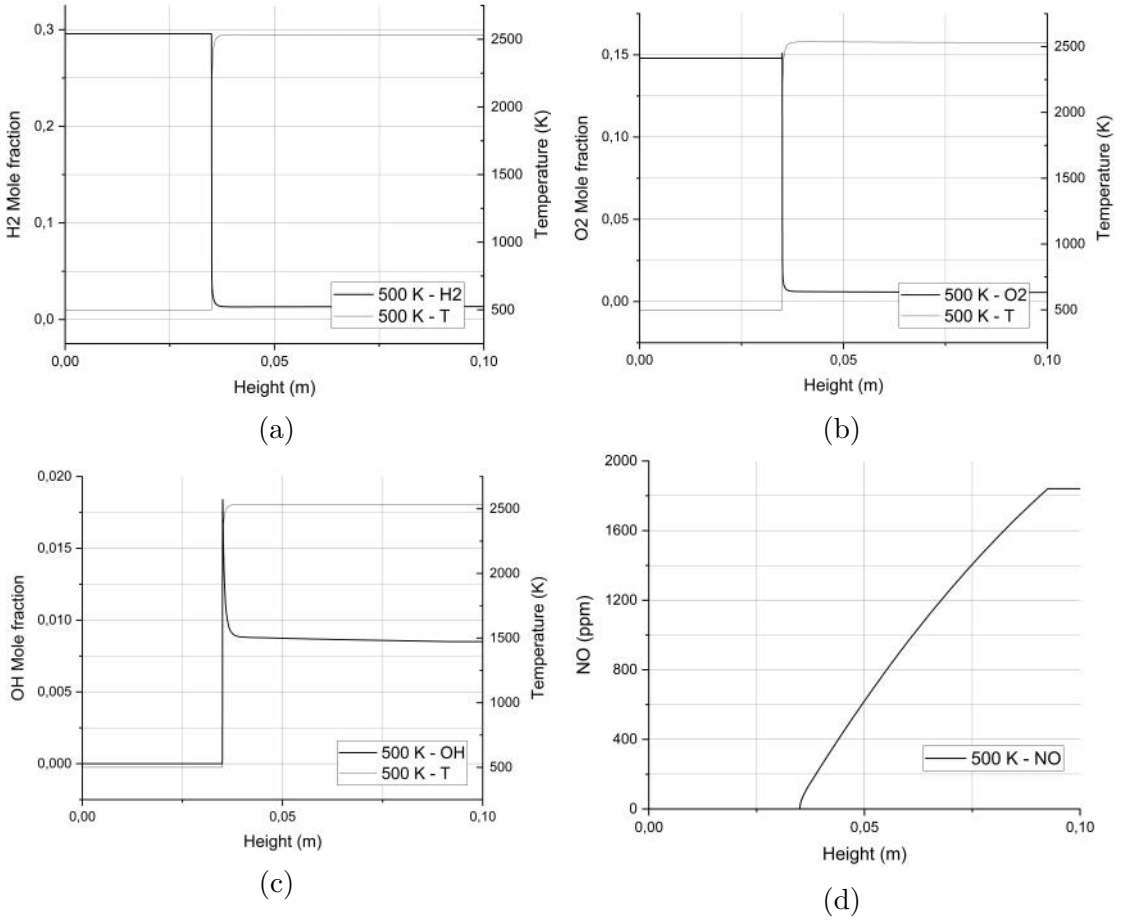

Figure A6: Extensive Analysis 500 K

Temperature Effect:

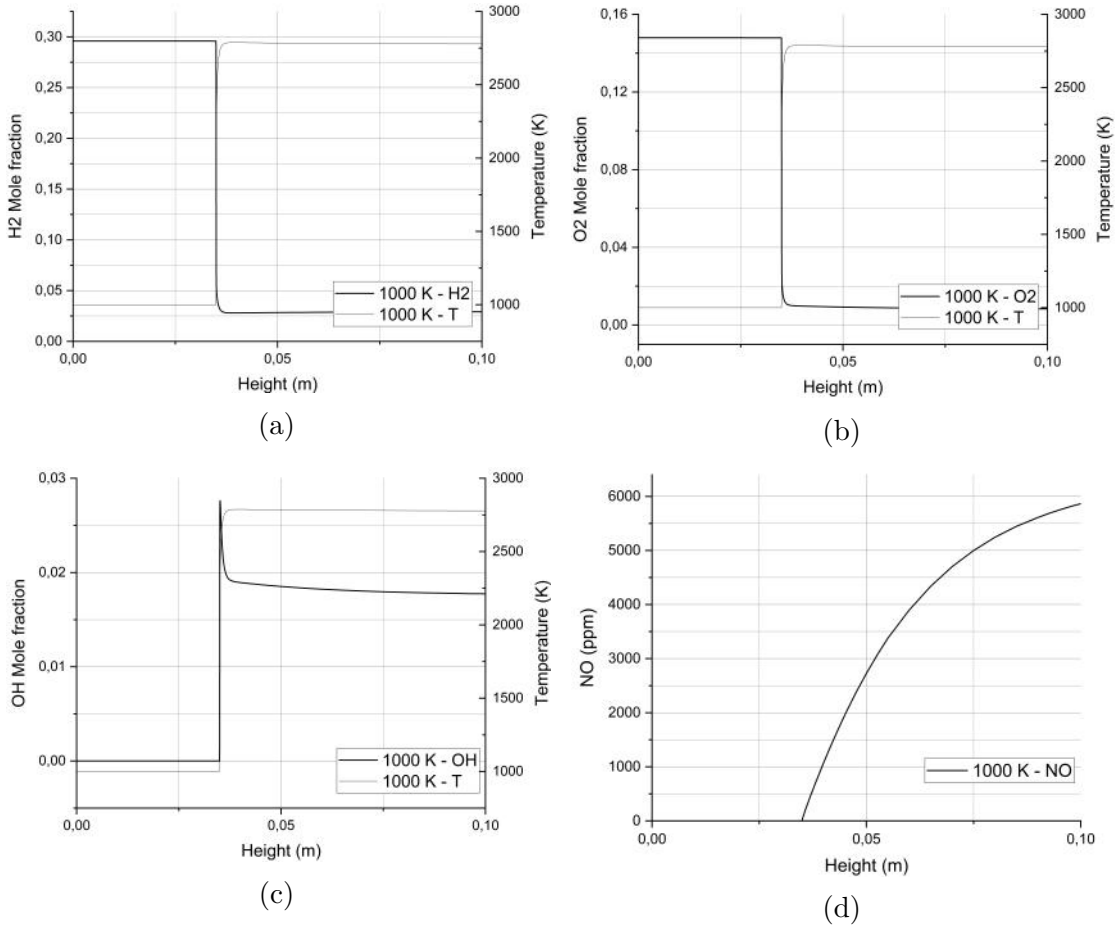

Figure A7: Extensive Analysis 1000 K

Experimental Setup:

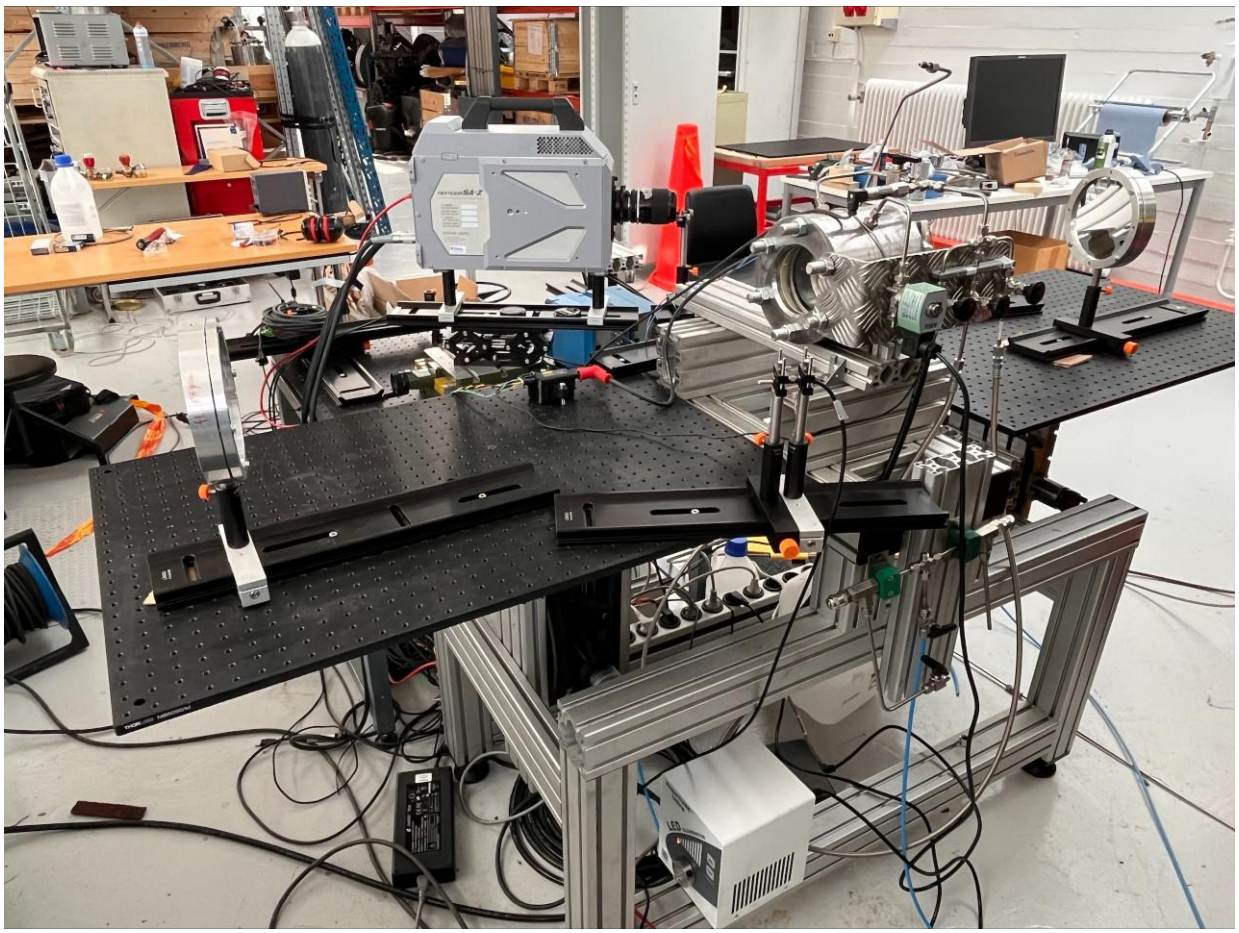

Figure A8: Experimental Setup

Overview Experimental Results:

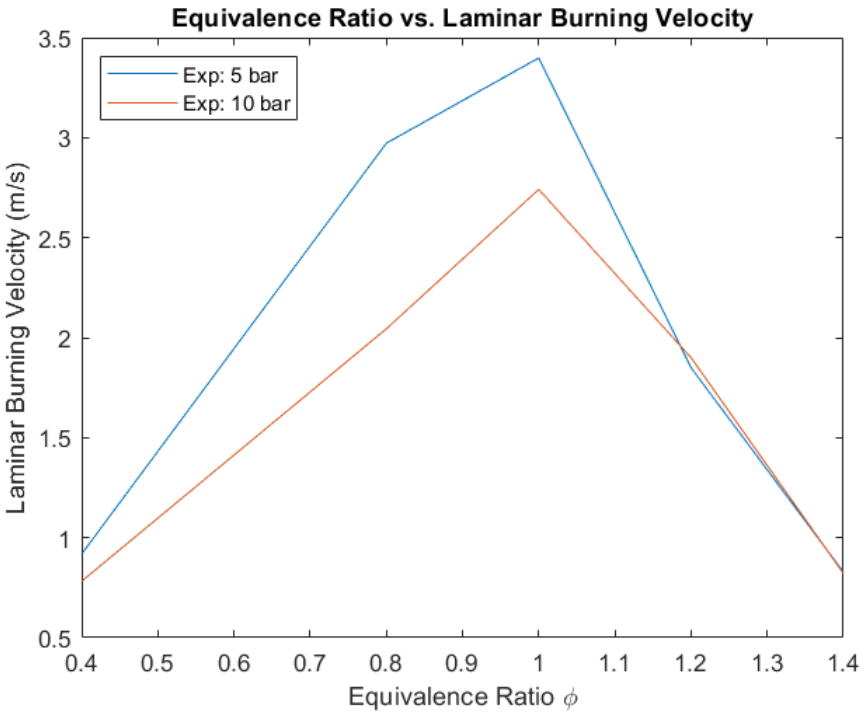

Figure A9: Comparison of Equivalence Ratio vs. Flame Speed - Conditions: T = 300 K, P = as stated, ϕ = 1.0, Dilution = 0 %